Journal of Medicinal Chemistry

pubs.acs.org/jmc

Article

Discovery of 5,6-Bis(4-methoxy-3-methylphenyl)pyridin-2-amine as a WSB1 Degrader to Inhibit Cancer Cell Metastasis

Jinxin Che, Zegao Jin, Fangjie Yan, Jieqiong You, Jiangfeng Xie, Binhui Chen, Gang Cheng, Hong Zhu, Qiaojun He, Yongzhou Hu, Bo Yang, Ji Cao,* and Xiaowu Dong*

Cite This: *J. Med. Chem.* 2021, 64, 8621−8643

Read Online

ACCESS | Metrics & More | Article Recommendations | Supporting Information

ABSTRACT: The gain of cell motility is an essential prerequisite for cancer metastasis. The ubiquitin ligase subunit WD repeat and SOCS box-containing 1 (WSB1) has been demonstrated to regulate hypoxia-driven tumor cell migration. However, there is still a lack of methods for discovering inhibitors targeting the WSB1 axis. Here, we employed phenotypic screening models and identified compound **4** that displayed migration inhibitory activity against WSB1-overexpressing cells. Further studies indicated that it may function as a WSB1 degrader, thus leading to the accumulation of the Rho guanosine diphosphate dissociation inhibitor 2 (RhoGDI2) protein, reversing the expression of downstream F-actin and formation of membrane ruffles, and disturbing the migration capacity of cancer cells. Moreover, compound **4** exhibited a promising *in vivo* anticancer metastatic effects. Our findings show the discovery of a new WSB1 degrader, providing a unique solution for the treatment of cancer metastasis.

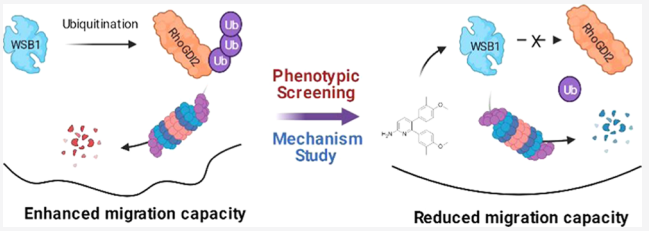

1. INTRODUCTION

As an important component of cancer development, cancer metastasis is characterized by the migration of cancer cells beyond the primary site where the tumor originated and eventually forming tumors in new sites (secondary and tertiary foci). Metastasis is generally untreatable and detrimental to cancer patients. Metastasis involves a multistep complex series of cell-biological events, termed as "invasion-metastasis cascade", including angiogenesis, detachment, migration, invasion, and adhesion.[1,2] Cancer metastasis is thought to be closely related to intratumoral hypoxia that contributes to the increased capacity of invasion and migration of tumor cells.[3,4] The signal pathways involved in the relationships between hypoxia and cell motility remain obscure.

WD repeat and SOCS box-containing 1 (WSB1) is a direct target of hypoxia-inducible factor 1 (HIF1), which helps tumor cells adapt to and survive in hypoxic conditions.[5] WSB1 forms an E3 ubiquitin ligase in complex with elongin B/C-Cullin5-Rbx1 and thus regulates tumor progression and chemoresistance through ubiquitination of multiple proteins such as the von Hippel-Lindau protein (pVHL),[6] ataxia-telangiectasia mutated kinase (ATM),[7] and homeodomain-interaction protein kinase 2 (HIPK2).[8] In our previous research,[9] WSB1 was found to be significantly upregulated under hypoxia and subsequently drove the metastatic potential in osteosarcoma cells. Moreover, the Rho guanosine diphosphate dissociation inhibitor 2 (RhoGDI2) level can be modulated by WSB1 through direct ubiquitination. RhoGDI2 is a potent inhibitor of Rho GTPases, which act as regulators of actin cytoskeletal organization and cell motility.[10−12] We demonstrated that the hypoxia-driven WSB1 promotes the proteasome-dependent degradation of RhoGDI2, thereby leading to an increased migration capacity of tumor cells.[9] Therefore, HIF-1α-WSB1-RhoGDI2 can be a novel branch of the HIF-1α signaling axis with anticancer potential by controlling the migration capacity of tumor cells (Figure 1). Besides, targeting the WSB1-RhoGDI2 pathway may overcome the nucleus escape of HIF-1α, providing new solutions for hypoxia-promoted cancer metastasis. However, apart from biological approaches such as gene mutation or silencing,[6−9] few small molecules have been reported to suppress tumor migration by interrupting the WSB1-RhoGDI2 pathway, which is crucial in clinical studies and the survival of patients with metastatic cancer.

Given that the crystal structure of the WSB1 protein has remained unsolved, and there is still a lack of screening models for identifying inhibitors targeting this pathway, it might not be easy to find active compounds modulating the WSB1−RhoGDI2 axis. Alternatively, phenotypic screening is a promising strategy for small-molecule drug discovery, especially for those lacking essential information on targets. To date, cell-based phenotypic screening of structurally diverse

Received: March 31, 2021
Published: June 1, 2021

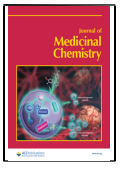

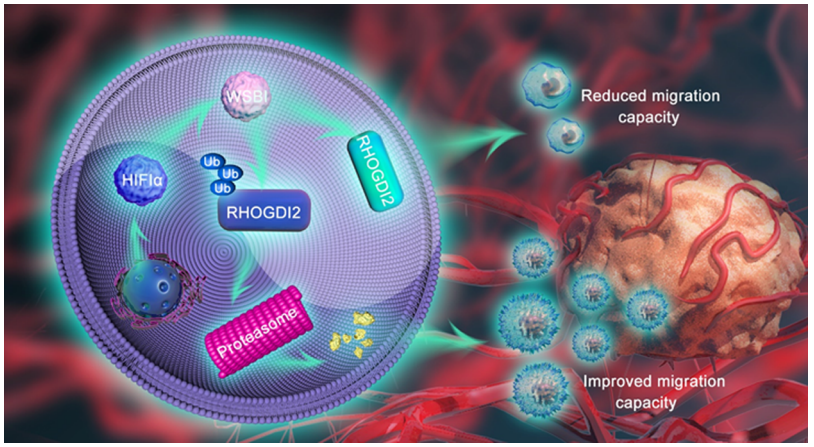

Figure 1. Function of the WSB1−RhoGDI2 axis.

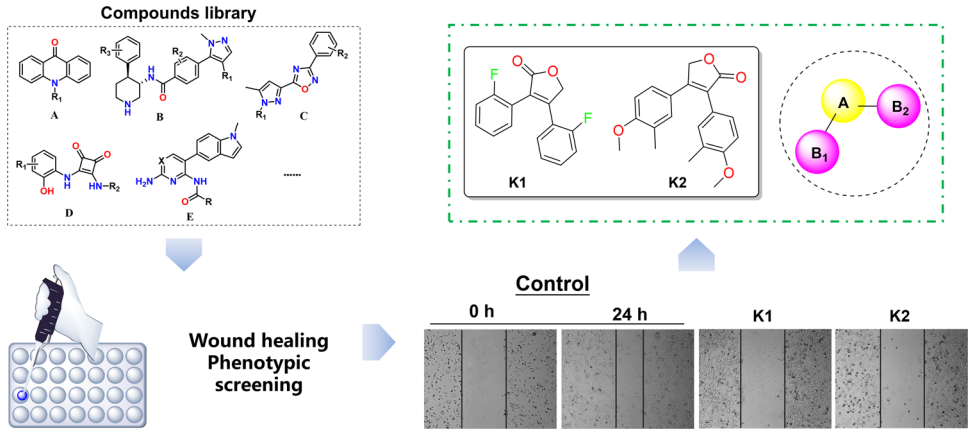

Figure 2. Discovery process of **K1** and **K2** with migration inhibitory activity.

compounds has delivered many hit/lead compounds.[13−16] As part of our continued interest in the area of phenotypic screening[17−19] and anticancer drug discovery,[20−22] the results of our further studies implied that the function of WSB1 promoting cell migration may not be cell-line-specific, so we started with the phenotypic function of compounds using wound-healing and transwell assay against different cell lines for the enrichment of compounds with antimigration potential. This was followed by a mechanism study to demonstrate whether the active compounds exert their effects through modulating the WSB1-RhoGDI2 signal pathway. In the present study, we report a new WSB1 degrader, compound **4** bearing the pyridin-2-amine scaffold, which can inhibit cancer cell metastasis *in vitro* and *in vivo*. This finding provides evidence that the hypoxia-driven metastasis of cancer can be inhibited through modulating the pathway and would help unleash the potential of the WSB1 protein as a therapeutic target.

2. RESULTS AND DISCUSSION

2.1. Identification of the Hit Compounds Based on Phenotypic Screening. First, the compounds from our in-house compound library were subjected to structural cluster analysis to avoid choosing compounds that bear the same scaffolds. After clustering, a total of 42 compounds bearing scaffolds A−N (Figure S1) were selected randomly for the following phenotypic screening. Their inhibitory effects against the migration of cancer cells were evaluated based on the wound-healing assay in human non-small-cell lung cancer (NSCLC) cells (H1299). Among them, the two compounds bearing scaffold K (furan-2(5*H*)-one), **K1** and **K2**, showed potent inhibitory activities against cancer cell migration at the concentration of 5 μM. The migration rates of cells treated with **K1** and **K2** were 0.51 ± 0.17 and 0.44 ± 0.07, respectively (Figure 2). Previously, only a few studies aimed to evaluate the antimigration potential of the compounds with the furan-2(5*H*)-one scaffold. This motivated us to use this new scaffold for further development of anticancer metastasis compounds. Structurally, **K1** and **K2** are composed of three different parts (Figure 2). Part **A** is a heterocycle system, while $\mathbf{B_1}$ and $\mathbf{B_2}$ are substituted phenyl rings. Furthermore, we derivatized **K1** and **K2** for preparing more potent compounds.

Compounds **1a−f**, **2a−g**, **3a−c**, and **4** were synthesized at first for a preliminary structure−activity relationship (SAR) study. The evaluation of the antimigration activity of such compounds was performed using a wound-healing assay against KHOS cells. The compounds that displayed good activity were chosen for further testing against H460 cells. Unless specifically mentioned, the wound-healing assay was performed under normoxia. For determining the concentration of the compounds in the wound-healing assay, the minimum toxic concentration of the synthesized compounds was evaluated. The results demonstrated that most of these compounds exhibit low cytotoxic activities (Table 1), so the test concentrations of compounds were set to 5 and 10 μM against KHOS and H460 cells, respectively.

https://doi.org/10.1021/acs.jmedchem.1c00586
J. Med. Chem. 2021, 64, 8621−8643

Table 1. Effects of Different Aryl Substituents on Cell Migration Activity

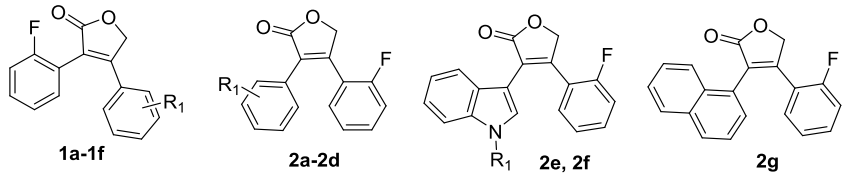

compound	R_1	KHOS cytotoxicity IC_{50} (μM)	KHOS cell migration rate[a]	H460 cytotoxicity IC_{50} (μM)	H460 cell migration rate[b]
1a	3-CH_3, 4-OCH_3	>50	0.47	>20	0.17
1b	4-F	>50	0.76	>20	0.91
1c	4-Cl	>50	0.70	N.T.[c]	N.T.
1d	4-$OCH(CH_3)_2$	>50	0.74	N.T.	N.T.
1e	3-CH_3, 4-$OCH_2CH_2CH_3$	>50	0.62	>20	0.54
1f	3-CH_3, 4-$OCH_2(CH_2)_3CH_3$	>50	N.A.[d]	N.T.	N.T.
2a	4-OCH_3	>50	0.80	>20	0.64
2b	4-OAc	>50	0.86	N.T.	N.T.
2c	4-F	>50	0.83	N.T.	N.T.
2d	4-CF_3	>50	0.73	N.T.	N.T.
2e	H	>50	N.A.	N.T.	N.T.
2f	$-CH_2CH_3$	>50	0.76	N.T.	N.T.
2g		>50	0.77	N.T.	N.T.

[a]The migration rate was normalized to the control: migration rate = $(C - D)/(A - B) \times 100\%$ (A = blank area of the control, 0 h; B = blank area of the control, 16 h; C = blank area of the compound, 0 h; D = blank area of the compound, 16 h). The tested concentration was 5 μM. The results are an average of three independent determinations. [b]The migration rate was normalized to the control: migration rate = $(C - D)/(A - B) \times 100\%$ (A = blank area of the control, 0 h; B = blank area of the control, 48 h; C = blank area of the compound, 0 h; D = blank area of the compound, 48 h). The tested concentration was 10 μM. The results are an average of three independent determinations. [c]N.T., not tested. [d]N.A., no activity; the average migration rate was >1.00.

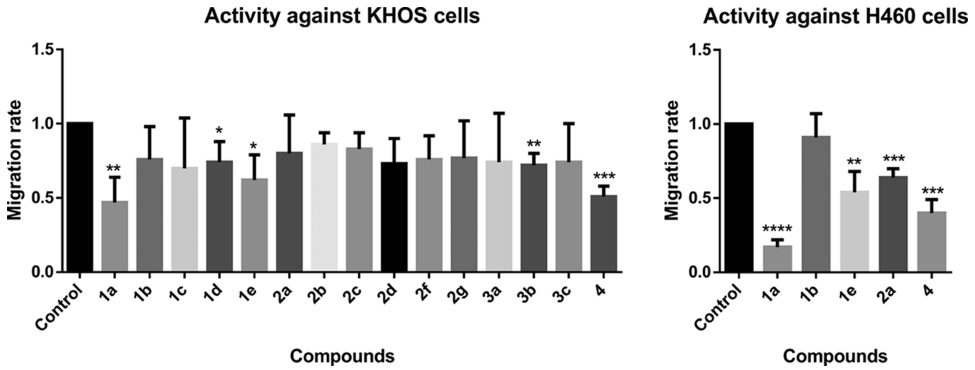

Figure 3. Migration rates of compounds **1a–4** against KHOS or H460 cells. The compounds with an average migration rate >1.00 are not shown. Results are shown as mean (n = 3) ± SD. *p < 0.05, **p < 0.01, ***p < 0.001 vs the control.

As shown in Table 1 and Figure 3, some of these compounds such as **1a**, **1d**, and **1e** showed significant activities in reducing the migration rate of KHOS cells. When the 3-position of the furan-2(5*H*)-one scaffold was 2-fluro phenyl (**1a–f**), the introduction of electron-withdrawing substituents on the 4-position aryl ring of the furan-2(5*H*)-one scaffold can lead to a decrease in activity (**1b**, **1c** vs **1a**). A loss of activity was observed when larger substituents such as the pentyloxy group were introduced (**1d**, **1e** vs **1f**). The modification of 2-fluro phenyl at the 3-position of the furan-2(5*H*)-one scaffold (**2a–d**) further reduced the migration inhibitory activity of the compounds. Moreover, the compounds in which the phenyl was changed to indol-3-yl (**2e** and **2f**) or naphthalin-1-yl (**2g**) failed to exhibit improved efficacy. The activities of compounds **1a**, **1d**, and **1e** against KHOS cells showed statistical significance (Figure 3). Further, some compounds that showed potency or no activity were tested and confirmed on H460 cells. The migration of H460 cells was significantly inhibited after treating with **1a**, **1e**, or **2a** (Figure 3). The combined results indicated that compound **1a** exhibited the most potent antimigration efficacy in both KHOS and H460 cell lines (photographs of wound healing are shown in Tables S1 and S2).

Considering the structure diversity requirement, compounds bearing similar scaffolds, 1*H*-pyrrole-2,5-dione and pyridin-2-amine, were further synthesized and evaluated (Table 2). Although compound **3b** exerted significant migration reduction activity against KHOS cells, the comparison between the compounds bearing the furan-2(5*H*)-one scaffold revealed that compounds with the 1*H*-pyrrole-2,5-dione scaffold (**3a–c**) did not exert an improved antimigration effect in KHOS and H460 cancer cell lines. Notably, when both R_1 and R_2 were 3-methyl-4-methoxyl substituted, compound **4** bearing the pyridine-2-amine scaffold exhibited the best efficacy, which was

https://doi.org/10.1021/acs.jmedchem.1c00586
J. Med. Chem. 2021, 64, 8621–8643

Table 2. Effects of Different Scaffolds on Cell Migration Inhibitory Activity

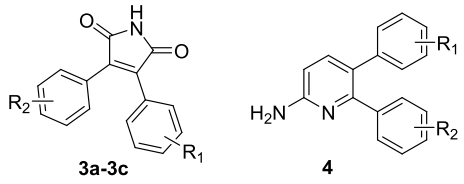

compound	R_1	R_2	KHOS cytotoxicity IC_{50} (μM)	KHOS cell migration rate[a]	H460 cytotoxicity IC_{50} (μM)	H460 cell migration rate[b]
3a	2-F	2-F	>50	0.74	>20	N.A.[d]
3b	4-OCH_3	2-F	>50	0.72	>20	N.A.
3c	3-CH_3, 4-OCH_3	2-F	>50	0.74	N.T.[c]	N.T.
4	3-CH_3, 4-OCH_3	3-CH_3, 4-OCH_3	39.1[a]	0.51	>20	0.40

[a]The migration rate was normalized to the control: migration rate = $(C - D)/(A - B) \times 100\%$ (A = blank area of the control, 0 h; B = blank area of the control, 16 h; C = blank area of the compound, 0 h; D = blank area of the compound, 16 h). The tested concentration was 5 μM. The results are an average of three independent determinations. [b]The migration rate was normalized to the control: migration rate = $(C - D)/(A - B) \times 100\%$ (A = blank area of the control, 0 h; B = blank area of the control, 48 h; C = blank area of the compound, 0 h; D = blank area of the compound, 48 h). The tested concentration was 10 μM. The results are an average of three independent determinations. [c]N.T., not tested. [d]N.A., no activity; the average migration rate was >1.00.

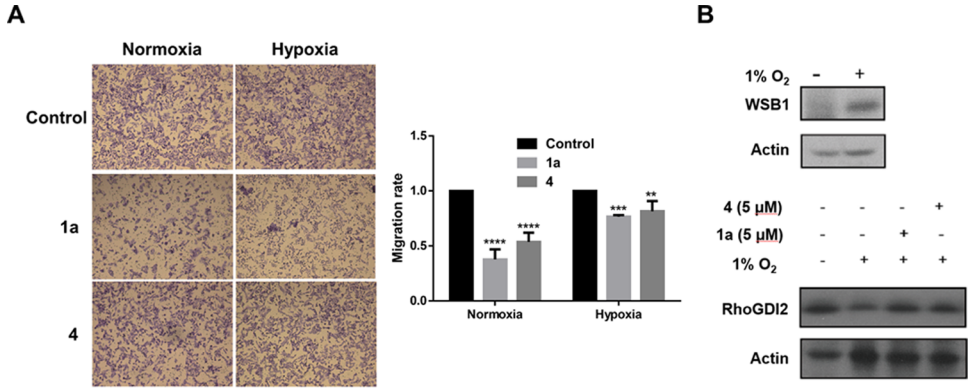

Figure 4. Compounds **1a** and **4** inhibited cell migration through elevating the levels of RhoGDI2 protein. (A) Transwell assay of compounds **1a** and **4** against KHOS cells under normoxia or hypoxia; the migration rate was normalized to the control: migration rate = A/B (A = number of migration cells in the dosing group; B = number of migration cells in the control group). (B) Western blotting of WSB1, RhoGDI2 in KHOS cells treated with compounds **1a** and **4** under hypoxia. Results are shown as mean (n = 3) ± SD. $^{**}p < 0.01$, $^{***}p < 0.001$, $^{****}p < 0.0001$ vs control.

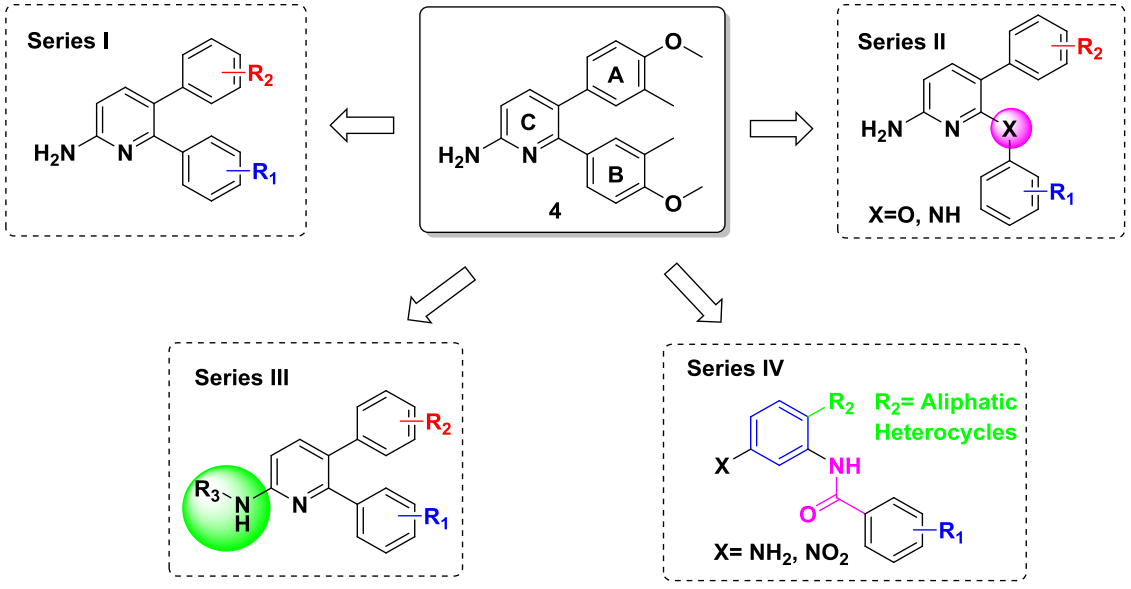

Figure 5. SAR exploration of compound **4**.

https://doi.org/10.1021/acs.jmedchem.1c00586
J. Med. Chem. 2021, 64, 8621−8643

comparable to compound **1a** (Figure 3; photographs of wound healing are shown in Tables S1 and S2). Therefore, compounds **1a** and **4** were chosen for the following optimization and mechanism study after the initial SAR exploration.

2.2. Compounds 1a and 4 May Function through Regulating the WSB1-RhoGDI2 Signal Pathway. In addition to the wound-healing assay, the antimigration activities of compounds **1a** and **4** were validated using a transwell assay. The results showed that both compounds also displayed good inhibitory potential under normoxia, with average cell migration rates of 0.38 and 0.54, respectively (Figure 4A). Moreover, it was found that compounds **1a** and **4** also significantly inhibited cancer cell migration under hypoxia (Figure 4A), with average cell migration rates of 0.77 and 0.82, respectively. This effect was comparable to their inhibitory potential under normoxia.

Since we have noticed the critical role of WSB1-RhoGDI2 in hypoxia-driven cancer metastasis, it motivated us to test whether compound **1a** or **4** could function through modulating the WSB1-RhoGDI2 pathway. WSB1 can ubiquitylate the RhoGDI2 protein and promote its proteasomal degradation, thereby stimulating the tumor cell motility and invasion. Our previous study demonstrated that the overexpression of RhoGDI2 could reverse the metastasis of osteosarcoma cells.[9] Therefore, the effects of compounds **1a** and **4** on the WSB1-RhoGDI2 signaling pathway were evaluated. The WSB1 protein quantity was significantly upregulated in KHOS cells under hypoxia, leading to a decrease in the RhoGDI2 protein (Figure 4B). On the other hand, the treatment with **1a** or **4** elevated the levels of the RhoGDI2 protein in cells. The results suggest that compounds **1a** and **4** may inhibit the migration of cancer cells through the WSB1−RhoGDI2 axis, which are worth further exploring.

2.3. *In Vitro* Antimetastasis Activity Evaluation of Pyridin-2-amine Derivatives. According to the preliminary SAR and mechanism study, pyridin-2-amine was selected as a privileged scaffold for inhibiting the ubiquitin function of WSB1 to prevent cancer cell metastasis. To fully understand the SAR of pyridin-2-amine derivatives and find more potent antimigration compounds that act as WSB1-RhoGDI2 modulators, we designed four series of compounds on the structural basis of compound **4** (Figure 5). Regarding series I, the substituents on A and B aryl rings were studied. Series II and III were designed to improve the metabolic properties of **4** while maintaining its antimigration activity. From the perspective of structure diversity, compounds with a skeleton similar to **4** were also investigated, such as series IV. During the following study, H460 cells were used to evaluate the migration activity of the compounds. The cytotoxic IC_{50} of each compound was tested before determining the tested concentration of compounds in the wound-healing assay.

As shown in Table 3, compounds with various substituents on the phenyl rings were synthesized and tested. Most compounds such as **5b−f** showed low cytotoxicity against H460 cells except for compound **5a**, which exhibited an IC_{50} value of 0.367 μM. The migration inhibitory activities of the compounds were tested at a concentration of 10 μM; compound **5a** was excluded because of its high cytotoxicity. The results indicate that the cells treated with compounds **5b** and **5c** showed a significant decrease in migration rates (Figure 6). The activities of compounds **5b−f** were lower than that of compound **4**. Compounds with substituents altered on the B ring showed better activities than that altered on the A ring (**5b** vs **5e**, **5c** vs **5f**).

Table 3. *In Vitro* Cell Migration Inhibitory Activity of Compounds 5a−f

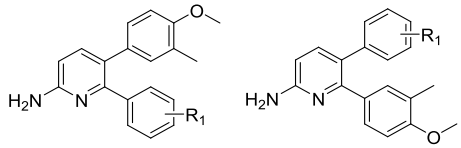

compound	R_1	cytotoxicity IC_{50} (μM)	migration rate[a]
5a	H	0.367	N.T.[b]
5b	4-$OCH(CH_3)_2$	13.7	0.67
5c	4-CF_3	26.13	0.60
5d	H	>40	N.A.[c]
5e	4-$OCH(CH_3)_2$	13.08	N.A.
5f	4-CF_3	21.7	0.91
4		24.47	0.48

[a]The migration rate was normalized to the control: migration rate = $(C - D)/(A - B) \times 100\%$ (A = blank area of the control, 0 h; B = blank area of the control, 48 h; C = blank area of the compound, 0 h; D = blank area of the compound, 48 h). The tested concentration was 10 μM. The results are an average of three independent determinations. [b]N.T., not tested. [c]N.A., no activity; the average migration rate was >1.00.

Further, heteroatoms such as nitrogen or oxygen were introduced between the pyridine scaffold and the B ring, which indicated that the original B ring was changed to phenoxyl or phenylamino substitution (Table 4). All of the compounds displayed low cytotoxicity against H460 cells, exhibiting IC_{50} values ranging from 2.58 to >40 μM. The migration inhibitory activities of the compounds were tested at a concentration of 10 μM; compound **6c** was excluded because of its high cytotoxicity. Among the compounds, compounds **6h**, **6j**, and **6l** displayed statistical significance in inhibiting the migration of cancer cells (Figure 6). Regarding phenoxyl substitution, all compounds exhibited a loss of activity (**6a**, **6b**, **6d−f**), irrespective of the substituents on the phenyl. Regarding phenylamino substitution, removal of substituents on the A ring resulted in a loss of the activity of compound **6g**. Substituent change of the A ring led to a decreased potency of the compounds **6h** and **6i** vs **4**, except for compound **6j**, in which R_1 is 4-trifluoromethyl and exhibited comparable migration inhibitory activity to **4**. After changing the B ring to the phenylamino group, **6k** showed a dramatic loss in potency, but the activity of compound **6l** improved when introducing 4-isopropyl to the phenylamino group. Collectively, the introduction of heteroatoms did not show any improvement in the migration inhibitory activity of the compounds.

Moreover, the introduction of hydrophilic side chains to the amino groups caused the cytotoxicity of the compounds to remain at low levels (Table 5). Most compounds (**7a−c**, **7e**, and **7f**) showed significant migration inhibitory activity against the cancer cells except for compound **7d** (Figure 6). The migration inhibitory activities of **7b** and **7f** were comparable to that of **4**.

Furthermore, compounds **8a−i** sharing a similar skeleton to **4** were synthesized and evaluated (Table 6). The pyridin-2-amine scaffold was changed to nitrobenzene or aniline scaffold, and the original B ring was changed to aliphatic heterocycles

https://doi.org/10.1021/acs.jmedchem.1c00586
J. Med. Chem. 2021, 64, 8621−8643

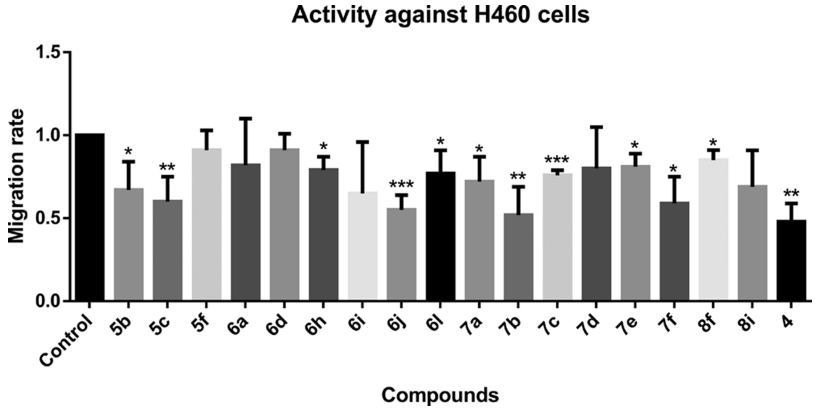

Figure 6. Migration rates of compounds **5b**−**8i** against H460 cells. The compounds with an average migration rate >1.00 are not shown. Results are shown as mean (n = 3) ± SD. *p < 0.05, **p < 0.01, ***p < 0.001 vs control.

Table 4. *In Vitro* Cell Migration Inhibitory Activity of Compounds 6a−l

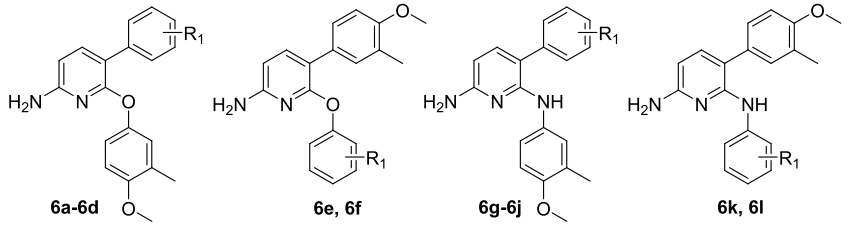

compound	R_1	cytotoxicity IC_{50} (μM)	migration rate[a]
6a	H	>40	0.82
6b	4-$OCH(CH_3)_2$	29.1	N.A.[b]
6c	3-CH_3, 4-OCH_3	2.58	N.T.[c]
6d	4-CF_3	15.9	0.91
6e	H	>40	N.A.
6f	4-$OCH(CH_3)_2$	>40	N.A.
6g	H	>40	N.A.
6h	4-$OCH(CH_3)_2$	33.4	0.79
6i	3-CH_3, 4-OCH_3	>40	0.65
6j	4-CF_3	11.4	0.55
6k	H	25.4	N.A.
6l	4-$OCH(CH_3)_2$	>40	0.77
4		24.47	0.48

[a]The migration rate was normalized to the control: migration rate = $(C - D)/(A - B) \times 100\%$ (A = blank area of the control, 0 h; B = blank area of the control, 48 h; C = blank area of the compound, 0 h; D = blank area of the compound, 48 h). The tested concentration was 10 μM. The results are an average of three independent determinations. [b]N.A., no activity; the average migration rate was >1.00. [c]N.T., not tested.

such as substituted piperidyl, piperazinyl, or morpholinyl. Although the compounds showed low cytotoxicity against H460 cells, the migration inhibitory rates suffered a dramatic loss. Although compounds **8f** and **8i** with morpholinyl substitution at R_2 displayed migration inhibitory activity, they performed worse than **4** (Figure 6).

2.4. Compounds Inhibit WSB1-Mediated Metastasis of Cancer Cells. To further address the effect of compounds on WSB1-manipulated cell metastasis, the inhibition of compounds on the metastasis of WSB1-overexpressing cells was evaluated. Compared with the empty plasmid pCDH-transduced KHOS cells (KHOS-pCDH), WSB1-overexpressing KHOS cells (KHOS-WSB1) enhanced the wound-healing capability of KHOS cells, indicating an efficient migrating potency of KHOS-WSB1 (Figure 7A). The wound-healing was not affected when the cells were treated with **7d**, but compound **4** can significantly block WSB1-enhanced wound healing of KHOS-WSB1 cells, exhibiting a low migration rate of 0.31 ± 0.10. A similar effect was observed in pCDH-transduced and WSB1-overexpressing H1299 cells. As shown in Figure 7B, the wound-healing of H1299-WSB1 cells was significantly inhibited by treating with compound **1a** or **4**. Notably, compound **1a** displayed lower migratory inhibitory potency than compound **4**.

Additionally, we further performed the transwell assay. As shown in Figure 7C, H1299-WSB1 cells migrated more efficiently into the lower chamber of the Transwell than H1299-pCDH cells. In line with the results from the wound-healing assay, the migrated capability of H1299-WSB1 cells was also blocked by compound **1a** or **4** (Figure 7C). To confirm the role of WSB1 in compound-mediated migration inhibition effect, we generated WSB1 knockout A2780 cells (A2780-WSB1/KO) by the crispr-cas9 technology. As expected, the A2780-WSB1/KO cells displayed a decrease in the wound-healing capability compared to wild-type A2780 (A2780-WT) cells (Figure 7D). Notably, compound **4** can

https://doi.org/10.1021/acs.jmedchem.1c00586
J. Med. Chem. 2021, 64, 8621−8643

Table 5. *In Vitro* Cell Migration Inhibitory Activity of Compounds 7a−f

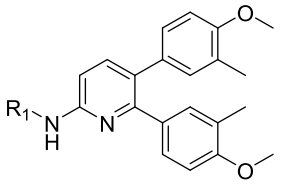

7a-7f

Compound	R_1	Cytotoxicity IC_{50} (μM)	Migration rate[a]
7a	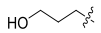	N.T.[b]	0.72
7b		18.5	0.52
7c	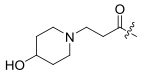	15.6	0.76
7d	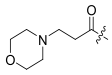	22.65	0.80
7e	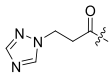	>40	0.81
7f	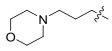	10.98	0.59
4	-	24.47	0.48

[a]The migration rate was normalized to the control: migration rate = $(C - D)/(A - B) \times 100\%$ (A = blank area of the control, 0 h; B = blank area of the control, 48 h; C = blank area of the compound, 0 h; D = blank area of the compound, 48 h). The tested concentration was 10 μM. The results are an average of three independent determinations. [b]N.T., not tested.

only block the wound-healing capability of wild-type A2780 (A2780-WT) cells but not the A2780-WSB1/KO cells (Figure 7D). Thus, these results clearly suggested that WSB1 could be a major knot for the function of compound **4**.

2.5. Compound 4 Is a WSB1 Degrader Increasing the RhoGDI2 Level. Next, we tried to explore the mechanism of compound-mediated migration inhibition. Accordingly, the effects of active compounds on the WSB1 signal pathway were evaluated. Some compounds that exhibited good or low migration inhibitory activity were chosen for incubating with the WSB1-transfected KHOS cells (KHOS-WSB1). As shown in Figure 8A, compounds such as **6a−c**, **6i**, **6k**, and **7d** that displayed no significant migration inhibition could not prevent the degradation of RhoGDI2 in cells. The quantity of RhoGDI2 protein increased after cells were incubated with the active compounds **6l** and **4**. However, compound **7f**, which showed good activities in H460 cells, did not exhibit the potential of modulating the WSB1-RhoGDI2 pathway, and the underlying mechanism still needs to be investigated. In this research, we mainly focused on compound **4**.

To confirm the way that the active compounds modulate the WSB1-RhoGDI2 signaling pathway, the H1299-WSB1 cell line was used to be treated with compounds **1a** and **4**. The result indicated that the WSB1-RhoGDI2 pathway was inhibited with a subsequent increase in the quantity of the downstream RhoGDI2 protein (Figure 8B), but compound **1a** showed a weaker activity than that of compound **4**. Interestingly, an obvious decrease in the level of the Myc-tagged WSB1 (Myc-WSB1) protein was seen after the cells were treated with compound **4**. When WSB1 was Flag-tagged, inhibition was also observed (Figure 8C). To investigate the mechanism of compound **4**-mediated WSB1 inhibition, we first explored the change of the mRNA level in H1299-WSB1 cells. The WSB1 mRNA level was 7.5-fold higher in H1299-WSB1 cells than that in H1299-pCDH cells, while the RhoGDI2 mRNA level was not influenced (Figure S2). After H1299-WSB1 cells were treated with compound **4**, the mRNA levels of RhoGDI2 and WSB1 displayed no change compared to that of untreated cells (Figure 8D), which indicated that the change in protein levels induced by compound **4** might not function through manipulating the mRNA level.

Next, we asked whether compound **4** affected the stability of WSB1. To address this, **MG123** (a proteasome degrader) and Chloroquine (**CQ**, a lysosomal inhibitor) were utilized (Figure 8C). It was found that **MG132** can prevent the compound **4**-induced degradation of WSB1 and lead to a comparable level of WSB1 to that in untreated cells without affecting the improvement of the RhoGDI2 level. However, **CQ** displayed no influences on the protein levels of WSB1 and RhoGDI2. These results suggested that compound **4** may induce WSB1 degradation in a proteasome-dependent manner. To confirm this, a time-dependent degradation effect of compound **4** against WSB1 was investigated (Figure 8E). Cycloheximide (**CHX**) was employed as a positive control, and a time-dependent decreased level of WSB1 was observed when cells were treated with compound **4**, which suggested that compound **4** may be a degrader of the WSB1 protein. Further, we evaluated the dose-dependent effect of compound **4**. As shown in Figure 8F, with the concentration of compound **4** decreased, so did the degradation effect. Moreover, we

https://doi.org/10.1021/acs.jmedchem.1c00586
J. Med. Chem. 2021, 64, 8621−8643

Table 6. *In Vitro* Cell Migration Inhibitory Activity of Compounds 8a−i

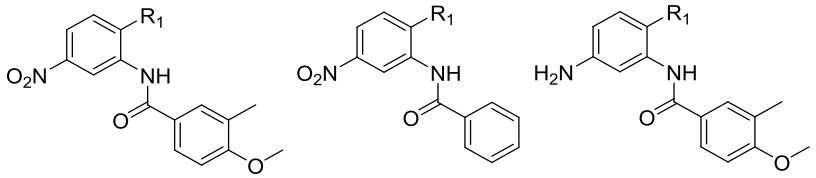

Compound	R_1	Cytotoxicity IC_{50} (μM)	Migration rate[a]
8a		>40	N.A.[b]
8b		>40	N.A.
8c		>40	N.A.
8d		>40	N.A.
8e		>40	N.A.
8f		>40	0.85
8g		>40	N.A.
8h		>40	N.A.
8i		>40	0.69
4	-	24.47	0.48

[a]The migration rate was normalized to the control: migration rate = $(C - D)/(A - B) \times 100\%$ (A = blank area of the control, 0 h; B = blank area of the compound, 0 h; C = blank area of the compound, 48 h; D = blank area of the compound, 48 h). The tested concentration was 10 μM. The results are an average of three independent determinations. [b]N.A., no activity; the average migration rate was >1.00.

generated the Flag-tagged green fluorescent protein (Flag-GFP) stably expressed H1299 cells. Compound **4** did not affect the protein level of Flag-GFP dose-dependently, which suggested that compound **4** induced the degradation of WSB1 rather than the Flag-tag.

To determine whether compound **4** can interact with WSB1 directly, we tried efforts to purify the WSB1 protein using the affinity chromatography method for *in vitro* binding experiments. However, it was found that the GST- or His-tagged WSB1 protein showed unexpected physicochemical properties. They were unstable and easily precipitated out at high concentrations (Figure S3), thereby being hard to be purified. Then, the interaction was further investigated by immunoprecipitation (Figure 8G). WSB1 and RhoGDI2 were coprecipitated from 293T cells overexpressing both proteins. However, compound **4** cannot block the coprecipitation of the proteins at different concentrations. The results indicated that compound **4** may not interact with the WSB1 protein directly.

Taken together, our results demonstrated that compound **4** may function through inducing the degradation of WSB1 in a proteasome-dependent manner, thus leading to the accumulation of the RhoGDI2 protein and subsequently lowering the migration capacity of cancer cells (Figure 8H).

2.6. Compound 4 Decreases the WSB1-Enhanced Expression of Downstream Polymerized Actin. Our previous findings indicated that WSB1-triggered RhoGDI2 suppression activates Rho GTPases.[9] RhoGDIs modulate the cycling of Rho GTPases between active or inactive states; Rho GTPases are known as regulators of actin cytoskeletal organization and motility of cells.[23] Since compound **4** was demonstrated as a degrader of WSB1, we examined the effect of compound **4** on the status of downstream polymerized actin (F-actin) organization in H1299-WSB1 cells. As illustrated in Figure 9, overexpression of WSB1 enhanced the fluorescence intensity of F-actin in cells, and the appearance of membrane ruffles was observed, indicating abundant F-actin expression and the cell motility ability was enhanced. Notably, after the cells were treated with compound **4**, the fluorescence intensity of F-actin and the formation of membrane ruffles decreased. These results suggest that the WSB1 degrader, compound **4**, can reverse the WSB1-driven expression of downstream F-actin and the formation of membrane ruffles and consequently abrogate cell motility and migration.

2.7. Pharmacokinetic Study. Compound **4** was selected for the *in vivo* pharmacokinetic studies in rats. After 100 mg/kg oral dosing or 160 mg/kg intraperitoneal dosing of compound **4**, the two ways of administration were observed with quick absorption (T_{max}), but the former dosing displayed a fast clearance ($T_{1/2}$). Moreover, C_{max} and AUC_{0-t} values of compound **4** in oral or intraperitoneal dosing groups showed acceptable blood exposure (Table 7). Therefore, compound **4** was suitable for *in vivo* efficacy studies.

2.8. Compound 4 Can Inhibit Metastasis of Cancer Cells *In Vivo*. To test whether the migration inhibitory effect could be reproduced *in vivo*, compound **4** was further evaluated using the Balb/c (nu/nu) mice model bearing highly metastatic 4T1 breast cancer cells. Paclitaxel was used as a positive control (10 mg/kg ip twice a week). The treatment

https://doi.org/10.1021/acs.jmedchem.1c00586
J. Med. Chem. 2021, 64, 8621−8643

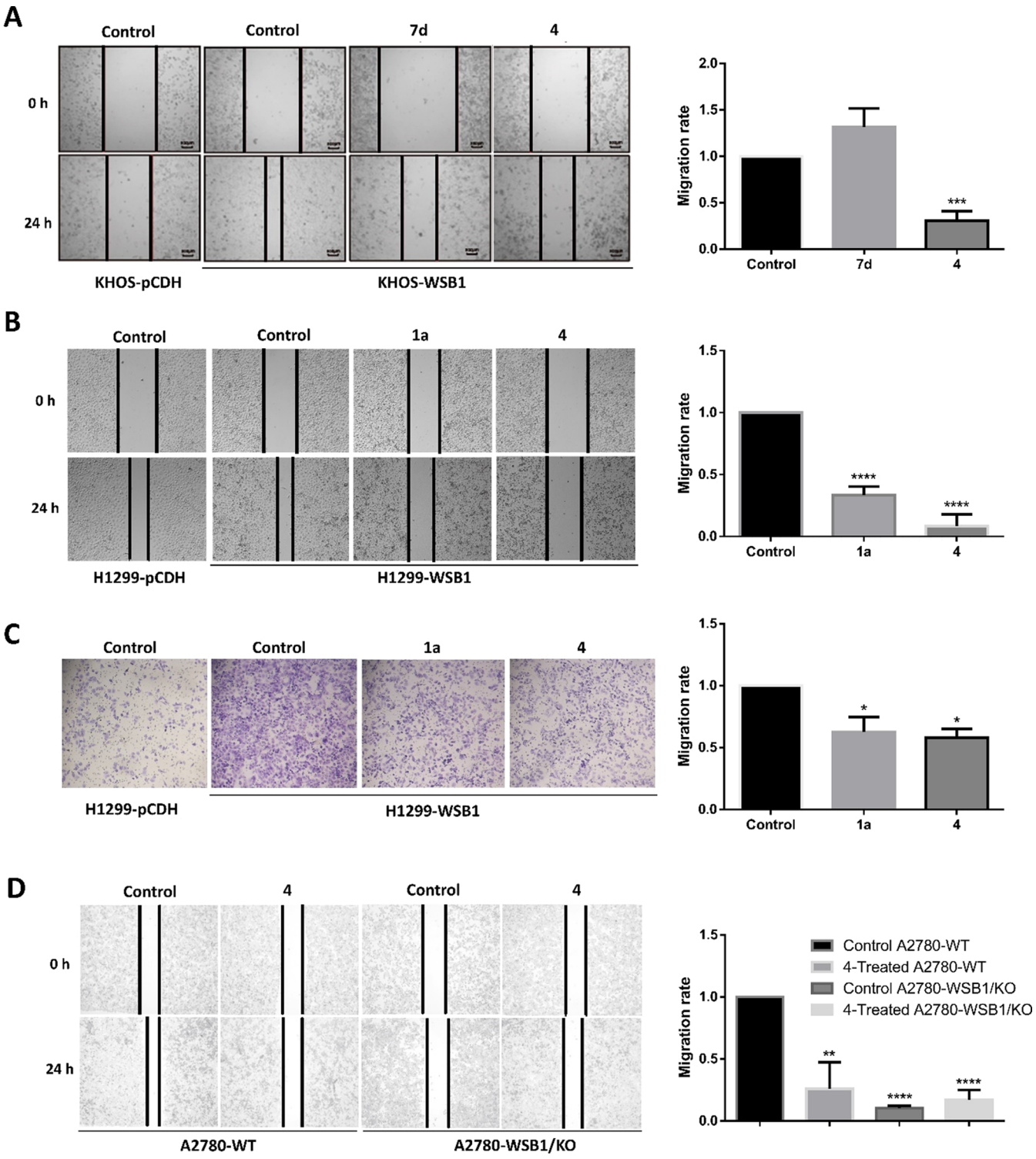

Figure 7. Compounds inhibited WSB1-mediated metastasis of cancer cells. (A) Images of the wound-healing assay of compounds **7d** and **4** against KHOS-pCDH and KHOS-WSB1 cells. (B) Images of the wound-healing assay and the transwell assay (C) of compounds **1a** and **4** against H1299-pCDH and H1299-WSB1 cells. (D) Images of the wound-healing assay of compound **4** against A2780-WT or A2780-WSB1/KO cells. Results are shown as mean (n = 3) ± SD. *p < 0.05, **p < 0.01, ***p < 0.001, ****p < 0.0001 vs control.

with compound **4** (po, 100 mg/kg/day) showed a comparable tumor inhibition and safety profile to paclitaxel (Figure 10A–C). Lungs from the tumor-bearing mice were excised for assessing metastasis. As shown in Figure 10D, the lungs of the untreated animals had 14.3 ± 9.0 colonies compared to only 5.7 ± 1.2 colonies in the animals treated with compound **4**, although the result showed no statistical significance. The results suggest that compound **4** can effectively inhibit the pulmonary metastasis of cancer cells.

2.9. Chemistry. The synthetic routes for the compounds **1a–f**, **2a–g**, and **3a–c** are outlined in Scheme 1. At first, the bromoacetophenone derivatives **10a–f** were synthesized via

https://doi.org/10.1021/acs.jmedchem.1c00586
J. Med. Chem. 2021, 64, 8621–8643

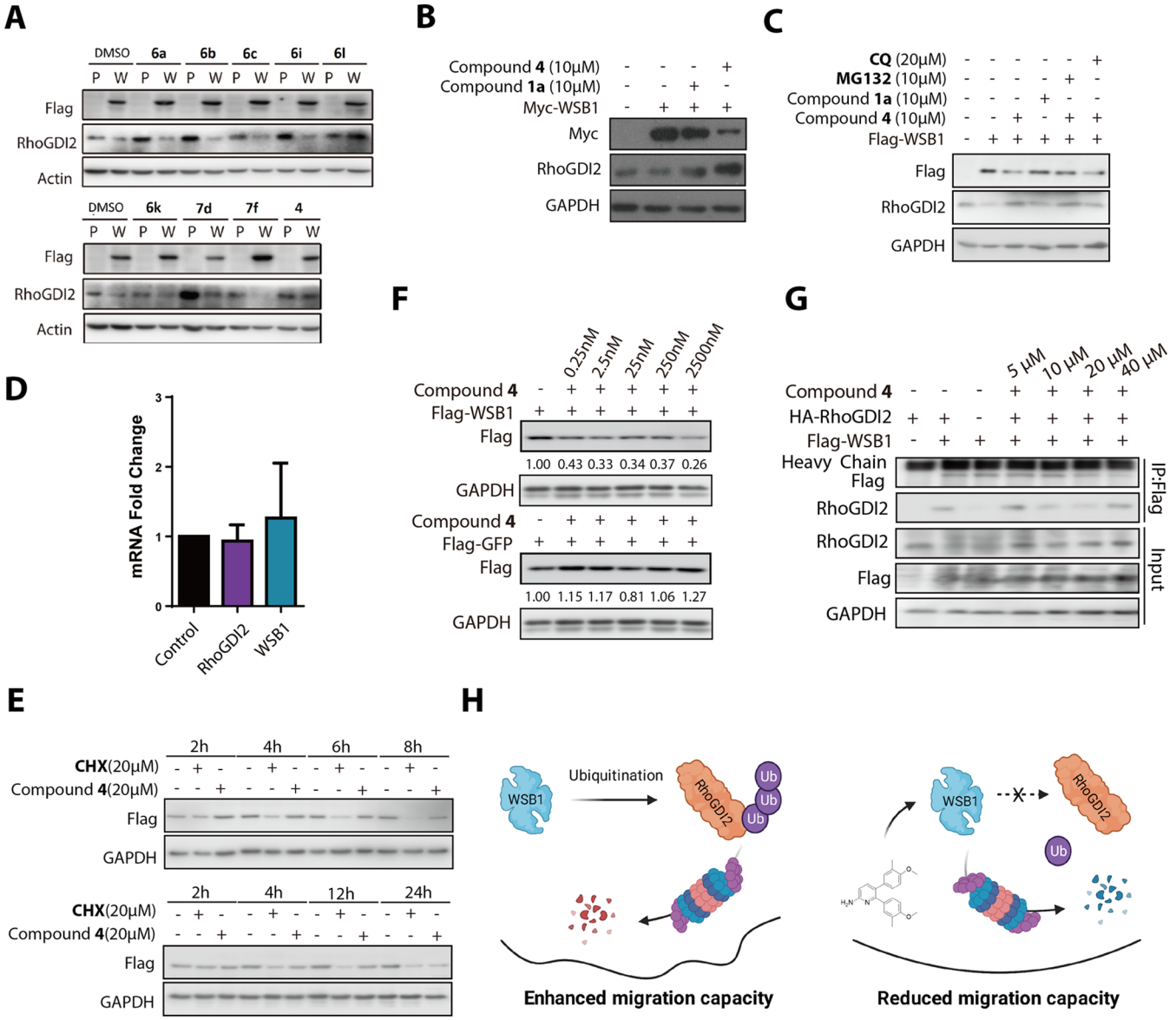

Figure 8. Compound **4** functions as a WSB1 degrader. (A) Western blotting of Flag-tag and RhoGDI2 in pCDH (P)- or WSB1 (W)-transfected KHOS cells treated with indicated compounds. (B, C) Western blotting of Myc-tag, Flag-tag, and RhoGDI2 in H1299-WSB1 cells treated with indicated compounds. (D) Relative mRNA levels of RhoGDI2 and WSB1 in H1299-WSB1 cells treated with compound **4**. The mRNA expression was analyzed by real-time polymerase chain reaction (RT-PCR) and shown as a histogram after normalization; GAPDH was used as a control gene. (E) Time-dependent and (F) dose-dependent degradation of Flag-WSB1 or Flag-GFP in H1299-WSB1 cells as indicated by Western blotting of Flag-tag. (G) Interaction between WSB1 and RhoGDI2. 293T cells transfected with Flag-WSB1 and RhoGDI2 plasmids, followed by compound **4** treatment. Cell lysates were immunoprecipitated with the anti-Flag antibody, followed by immunoblotting with anti-Flag and anti-RhoGDI2 antibody. (H) Schematic view of the possible mechanism of compound **4** for inhibiting cancer cell metastasis.

the bromination of acetophenone **9a**–**f** using $CuBr_2$ in EtOAc. Then, the intermolecular condensation of **6a**–**f** and 2-(2-fluorophenyl)acetic acid delivered the cyclized products **1a**–**f**. Besides, 2-flurobromoacetophenone (**10**) was brominated to obtain the bromoacetophenone derivative **12**, which was further condensed with corresponding phenylacetic acids **13a**–**g** to receive cyclized products **2a**–**g**. Furthermore, compounds **K1**, **1a**, and **2a** were treated with a saturated ethanolic solution of ammonia, affording target compounds **3a**–**c**.

The synthetic routes for compounds **4** and **5a**–**f** are outlined in Scheme 2. Bromination of compound **14** or **17** using *N*-bromosuccinimide (NBS) afforded compound **15** or **18**, respectively. Subsequently, Suzuki coupling reaction with 2-(substituted phenyl)-4,4,5,5-tetramethyl-1,3,2-dioxaborolane was performed in the presence of $Pd(PPh_3)_4$ and a base to obtain compounds **16a**–**c** and **19**, which were then further coupled to afford the target products **4** and **5a**–**f**.

The synthetic routes for compounds **6a**–**l** are outlined in Scheme 3. A nucleophilic reaction of compound **20** with 2-iodine propane yielded the phenol intermediate **21**. Oxidation and hydrolysis of compound **22** produced the intermediate **23**. Coupling reaction of compound **15** using the CuI catalyst with different substituted phenols provided **24a**–**c**, which were then coupled with substituted phenylboronic acid to give the target compounds **6a**–**f**. The amino group of compound **15** was protected by condensation with pivaloyl chloride. As described above, there were two steps of the coupling reaction of compound **25** to give **26d**–**j** using $Pd(OAc)_2$ and Pd(dppf)-

https://doi.org/10.1021/acs.jmedchem.1c00586
J. Med. Chem. 2021, 64, 8621−8643

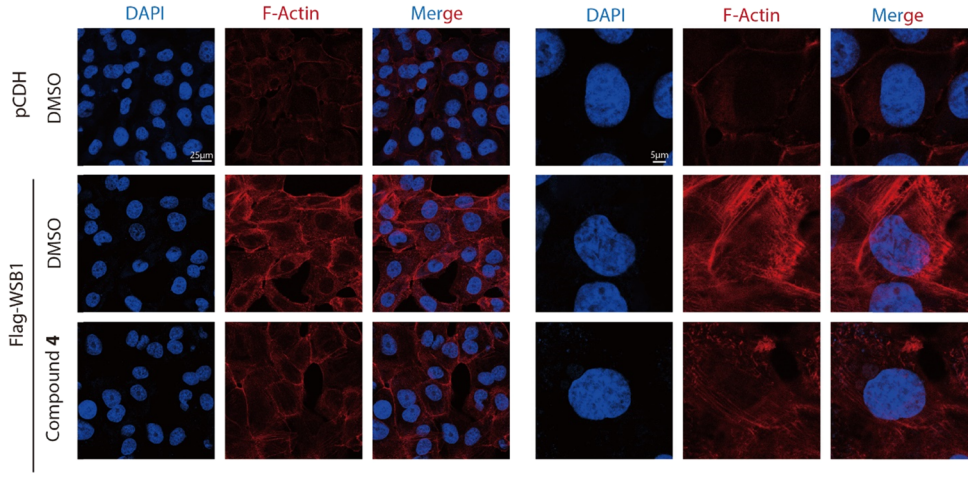

Figure 9. Representative images of the F-actin fluorescence intensity and the ruffles of H1299-WSB1 or H1299-pCDH cells treated with the indicated compounds.

Table 7. Pharmacokinetic Profiles of Compound 4

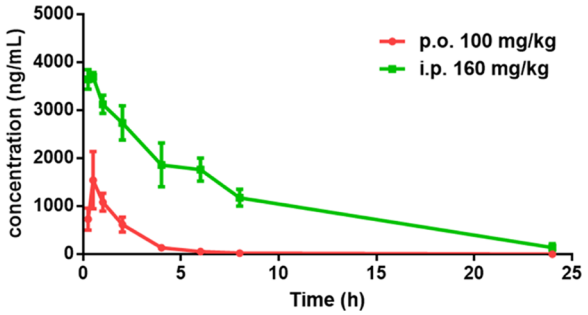

parameters	po	ip
T_{max} (h)	0.50 ± 0.01	0.42 ± 0.14
$T_{1/2}$ (h)	1.28 ± 0.31	4.97 ± 0.88
C_{max} (ng/mL)	1543 ± 595	3773 ± 120
AUC_{0-t} (ng/mL·h)	2898 ± 797	27 712 ± 4251
$AUC_{0-\infty}$ (ng/mL·h)	2941 ± 827	28 778 ± 5008

Cl_2, which were then deprotected to the target compounds **6g−l**.

The synthetic routes for compounds **7a−f** are outlined in Scheme 4. A nucleophilic reaction of compound **4** with allyl bromide gave compound **27**, which was subsequently oxidized to afford the target compounds **7a** and **7b**. Compound **28** was prepared by condensation of compound **4** with 3-chloropropionyl chloride, followed by nucleophilic reaction with various heterocycles to obtain compounds **7c−e**. A reduction reaction was performed to convert the amide **7d** to **7f**.

The synthetic routes for compounds **8a−i** are outlined in Scheme 5. Substituted benzoic acids **29a** and **29b** were condensed with 2-fluoro-5-nitroaniline, giving amide **31a** and **31b**. Substitution reaction was performed with different aliphatic heterocycles such as piperidin-4-ol, 1-methylpiperazine, and morpholine to afford target compounds **8a−f**. The nitryl in **8a−c** was reduced in the presence of Fe/NH_4Cl to get the target compounds **8g−i**.

3. CONCLUSIONS

Hypoxia-induced WSB1 expression can lead to the activation of the Rho pathway via RhoGDI2 depletion and consequently promote motility and migration of cancer cells. This increases the probability of tumor metastasis. The inhibition of this pathway may provide a new approach for suppressing hypoxia-driven cancer metastasis. However, essential structural information and screening models for WSB1 protein are still lacking. In this study, we employed a phenotypic screening method and discovered furan-2(5*H*)-one derivatives with potent antimigration efficacy. Further optimization and bioevaluation identified a series of pyridin-2-amine derivatives that displayed excellent *in vitro* efficacy. The migration rates of cells treated with active compounds range from 0.4 to 0.9. The compounds displaying significant anticancer cell migration effects were enriched.

A preliminary mechanism study disclosed that some of the active compounds can inhibit the migration capacity of WSB1-overexpressing cells. Compounds **1a**, **4**, and **6l** exert their antimigration effects by increasing the level of the RhoGDI2 protein. Further mechanism study indicated that compound **4** may induce WSB1 degradation through a proteasome-dependent manner without affecting the mRNA levels of WSB1 and RhoGDI2. Thus, this led to the accumulation of RhoGDI2 protein, subsequently lowering the migration capacity of cancer cells. For demonstrating the interaction between compound **4** and the WSB1 protein, although the purification of the WSB1 protein using affinity chromatography for *in vitro* binding experiments failed, immunoprecipitation showed that compound **4** had no influences on the WSB1−RhoGDI2 interaction, indicating that it may not interact with the WSB1 protein directly. The WSB1-driven expression of the downstream F-actin and formation of membrane ruffles in cancer cells can be reversed upon the treatment of compound **4**, suggesting that compound **4** displayed efficacies in modulating this pathway. Moreover, compound **4** showed promising pharmacokinetic profiles and an excellent effect in reducing the number of metastatic colonies *in vivo*. To our knowledge, compound **4** is the first reported WSB1 degrader, which would help unleash the potential of the WSB1 protein as a therapeutic target. In-depth mechanism exploration of the degrader is being carried out in our laboratory.

4. MATERIALS AND METHODS

4.1. Chemistry. All reagents and solvents were used as purchased from commercial sources. Chromatography was performed using silica gel (200−300 mesh). All reactions were monitored by thin-layer

https://doi.org/10.1021/acs.jmedchem.1c00586
J. Med. Chem. 2021, 64, 8621−8643

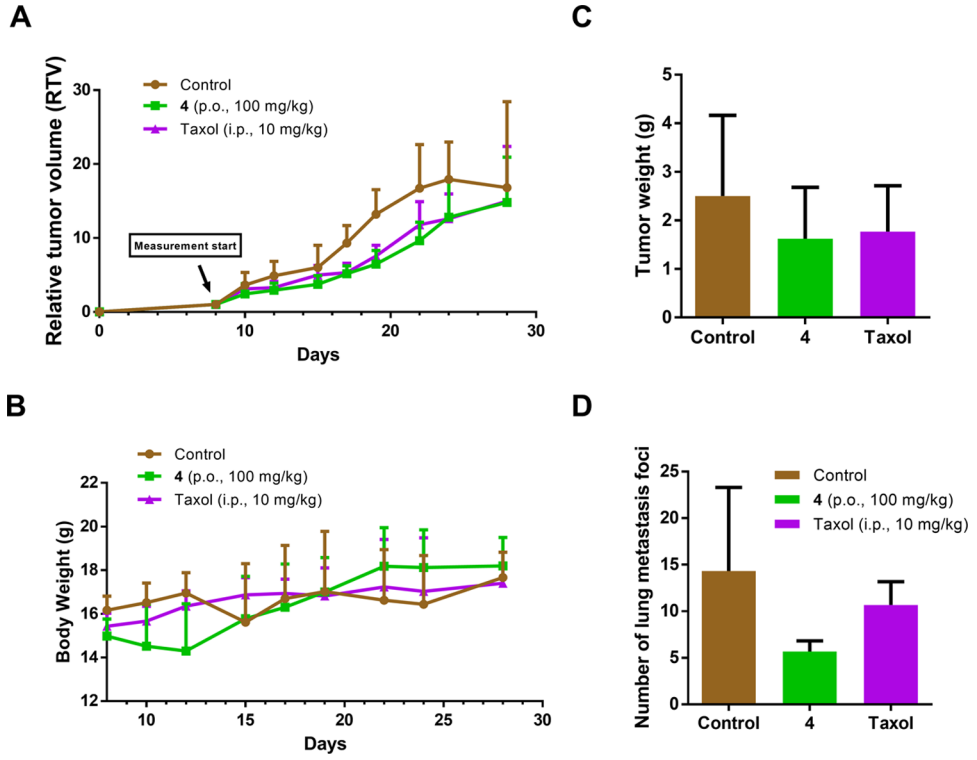

Figure 10. Treatment with compound **4** leads to decreased metastasis of tumor in the 4T1 xenograft mouse model. Tumor volume (A), body weight (B), tumor weight (C), and number of metastatic colonies (D) at indicated days for 28 days following treatment with compound **4** at indicated doses. Data represent the mean (n = 6) ± SD values.

Scheme 1. Synthetic Route for Target Compounds 1a–g, 2a–g, and 3a–c[a]

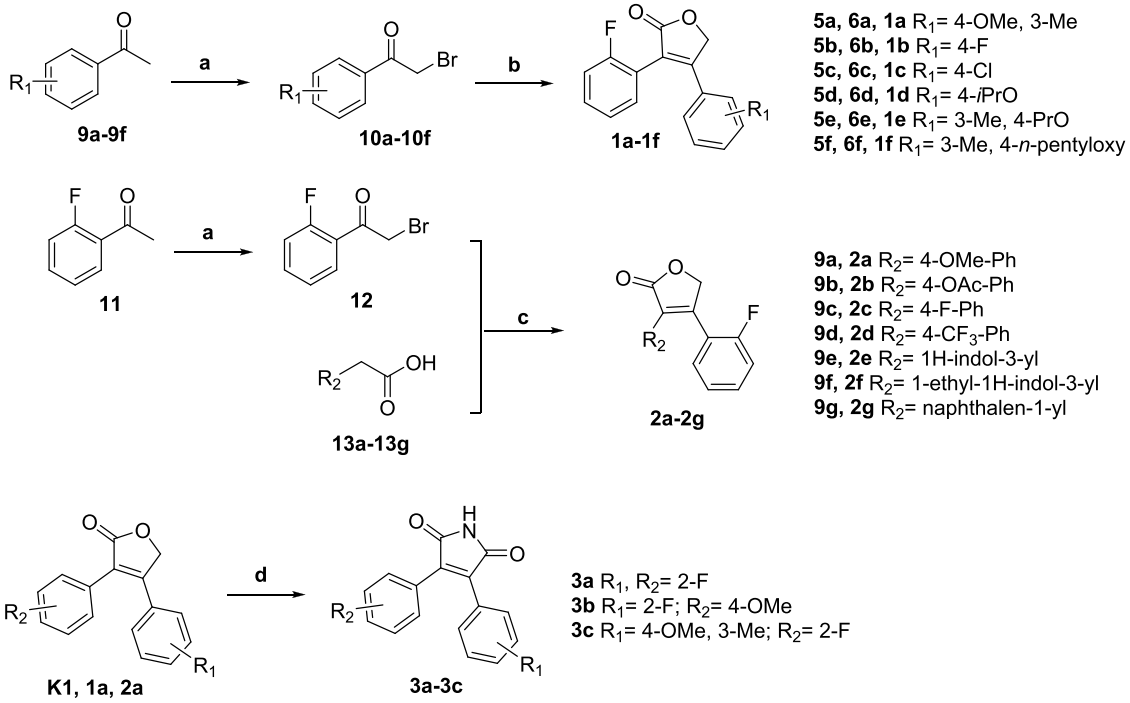

[a](a) Cu_2Br, ethyl acetate; (b) 2-(2-fluorophenyl)acetic acid, dimethylformamide (DMF); (c) i, triethylamine (TEA), MeCN; ii, 1,8-diazabicyclo[5.4.0]undec-7-ene (DBU), dichloromethane (DCM); (d) NH_3 saturated EtOH; (e) i, hexamethylenetetramine, DCM; ii, HBr, MeOH; (f) 2-(2-fluorophenyl)acetic acid, 1-hydroxybenzotriazole (HOBt), EDCI, DCM; (g) *t*-BuOK, *t*-BuOH.

chromatography (TLC), using silica gel plates with fluorescence F254 and UV-light visualization. ^{1}H NMR and ^{13}C NMR spectra were obtained on a Bruker Advance III 500 with the use of $CDCl_3$ or DMSO-d_6 as the solvent. Chemical shifts are referenced to the residual solvent peak and reported in ppm (d scale), and all coupling constant (J) values are given in hertz. Multiplicities are recorded by

https://doi.org/10.1021/acs.jmedchem.1c00586
J. Med. Chem. 2021, 64, 8621–8643

Scheme 2. Synthetic Route for Target Compounds 4 and 5a−f[b]

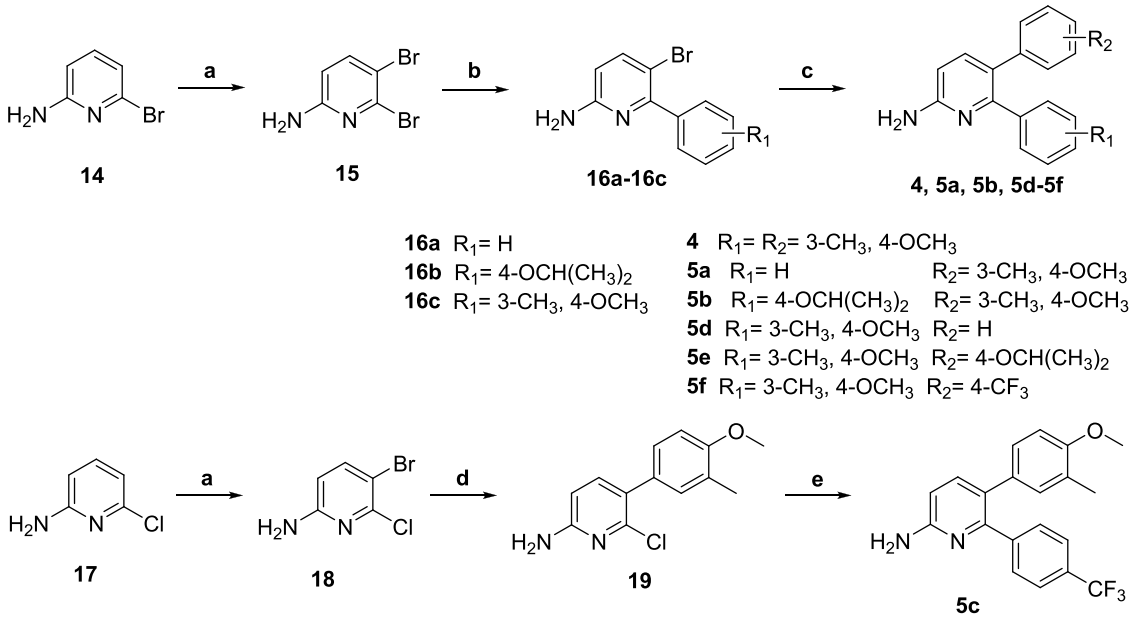

[b](a) NBS, DCM; (b) 2-(substituted phenyl)-4,4,5,5-tetramethyl-1,3,2-dioxaborolane, $Pd(PPh_3)_4$, Na_2CO_3, MeOH/H_2O/toluene = 1:25:10; (c) 2-(substituted phenyl)-4,4,5,5-tetramethyl-1,3,2-dioxaborolane, $Pd(PPh_3)_4$, Cs_2CO_3, H_2O/1,4-dioxane = 1:2; (d) 2-(4-methoxy-3-methylphenyl)-4,4,5,5-tetramethyl-1,3,2-dioxaborolane, $Pd(PPh_3)_4$, K_2CO_3, toluene/ethanol = 5:3; (e) 4,4,5,5-tetramethyl-2-(4-(trifluoromethyl)phenyl)-1,3,2-dioxaborolane, $Pd(OAc)_2$, Cs_2CO_3, XPhos, *n*-butyl alcohol.

the following abbreviations: s, singlet; d, double; t, triplet; q, quartet; m, multiplet; J, coupling constant (Hz). Electrospray ionization mass spectrometry (ESI-MS) data were recorded on a Shimadzu LC-MS 2020 instrument. Purity of all final compounds was ≥95% as determined by NMR and high-performance liquid chromatography (HPLC). The analytical HPLC was performed on an Agilent 1260 Infinity II (LC03) machine and a C18 reversed-phase column (Agilent Eclipse XDB-C18, 4.6 × 250 mm^2, 5 μm), with a flow rate of 1.0 mL/min, detection by UV absorbance at a wavelength of 254 nm, column temperature of 25 °C, and eluting with water (0.1% H_3PO_4) as A phase and acetonitrile as B phase (for 20 min elution time: 0 min, A phase: 90%, B phase: 10%; 15 min, A phase: 10%, B phase: 90%; 20 min, A phase: 5%, B phase: 95%; for 23 min elution time: 0 min, A phase: 55%, B phase: 45%; 8 min, A phase: 30%, B phase: 70%; 15 min, A phase: 10%, B phase: 90%; 23 min, A phase: 5%, B phase: 95%; for 25 min elution time: 0 min, A phase: 80%, B phase: 20%; 15 min, A phase: 10%, B phase: 90%; 20 min, A phase: 5%, B phase: 95%).

4.1.1. General Procedure A. To a solution of substituted acetophenone (compounds **9a−f** and **11**, 1 equiv) in ethyl acetate was added $CuBr_2$ (3.05 equiv); then, the mixture was refluxed overnight. After completion of the reaction, the mixture was filtered and washed with ethyl acetate. The combined organic layers were washed with 1 N hydrochloric acid and brine, dried over Na_2SO_4, and concentrated. The residue was purified by silica gel chromatography using 2% ethyl acetate in petroleum ether to afford compounds **10a−f** and **12**.

To the solution of substituted phenylacetic acid (compounds **13a−g**, 1 equiv) in MeCN (5 mL) were added substituted α-bromoacetophenone (compounds **10a−f** and **12**, 1 equiv) and triethylamine (0.3 mL). The mixture was stirred at room temperature for 0.5−4 h. Then, DBU (0.3 mL) was added and stirred at 0 °C for 0.3−8 h. After the solvent was removed, the residue was diluted with 1 N HCl and then extracted with ethyl acetate. The combined organic layers were washed with brine, dried over Na_2SO_4, and then concentrated under vacuum. The residue was purified by silica gel chromatography using 12% ethyl acetate in petroleum ether to afford compounds **1a−f** and **2a−g**.

4.1.2. General Procedure B. To a solution of compound **K1**, **1a**, or **2a** (0.36 mmol) was added ammonia saturated ethanol (3 mL) in a sealed bottle. Then, the mixture was heated to 110 °C for 6 h. After the reaction was completed, the reaction was cooled to room temperature and concentrated under vacuum. The residue was purified by silica gel chromatography using 1% methanol in dichloromethane to afford compound **3a−c**.

4.1.3. General Procedure C. To a solution of compound **15** (2 mmol), 2-(substituted phenyl)-4,4,5,5-tetramethyl-1,3,2-dioxaborolane (2 mmol) and Na_2CO_3 (4 mmol) in MeOH/H_2O/toluene = 10 mL:25 mL:10 mL were added $Pd(PPh_3)_4$ (0.06 mmol) under a N_2 atmosphere. Then, the mixture was heated to 85 °C for 4 h. After completion of this reaction, it was cooled to room temperature. The mixture was poured into 100 mL of cold water and extracted with ethyl acetate. The combined organic layers were washed with brine, dried over Na_2SO_4, and then concentrated under vacuum. The residue was purified by silica gel chromatography using ethyl acetate in petroleum ether (1:20) to afford compounds **16a−c**.

4.1.4. General Procedure D. To a solution of compounds **16a−c** (2 mmol), 2-(substituted phenyl)-4,4,5,5-tetramethyl-1,3,2-dioxaborolane (2.2 mmol) and Cs_2CO_3 (4 mmol) in H_2O/1,4-dioxane = 3 mL:6 mL were added $Pd(PPh_3)_4$ (0.06 mmol) under a N_2 atmosphere. Then, the mixture was heated to 85 °C for 8 h. After completion of this reaction, it was cooled to room temperature. The mixture was poured into 100 mL of cold water and extracted with ethyl acetate. The combined organic layers were washed with brine, dried over Na_2SO_4, and then concentrated under vacuum. The residue was purified by silica gel chromatography using ethyl acetate in petroleum ether (1:10−1:4) to afford compounds **4**, **5a**, **5b**, and **5d−f**.

4.1.5. General Procedure E. To a solution of compound **15** (9.64 mmol), substituted phenol (14.5 mmol), and TMEDA (0.55 mmol) in DMSO were added CuI (0.55 mmol) and Cs_2CO_3 (5.52 mmol) under a N_2 atmosphere. The mixture was heated to 100 °C and reacted overnight. The mixture was poured into 300 mL of cold water and extracted with ethyl acetate. The combined organic layers were washed with brine, dried over Na_2SO_4, and then concentrated under vacuum. The residue was purified by silica gel chromatography using

https://doi.org/10.1021/acs.jmedchem.1c00586
J. Med. Chem. 2021, 64, 8621−8643

Scheme 3. Synthetic Route for Target Compounds 6a–l[c]

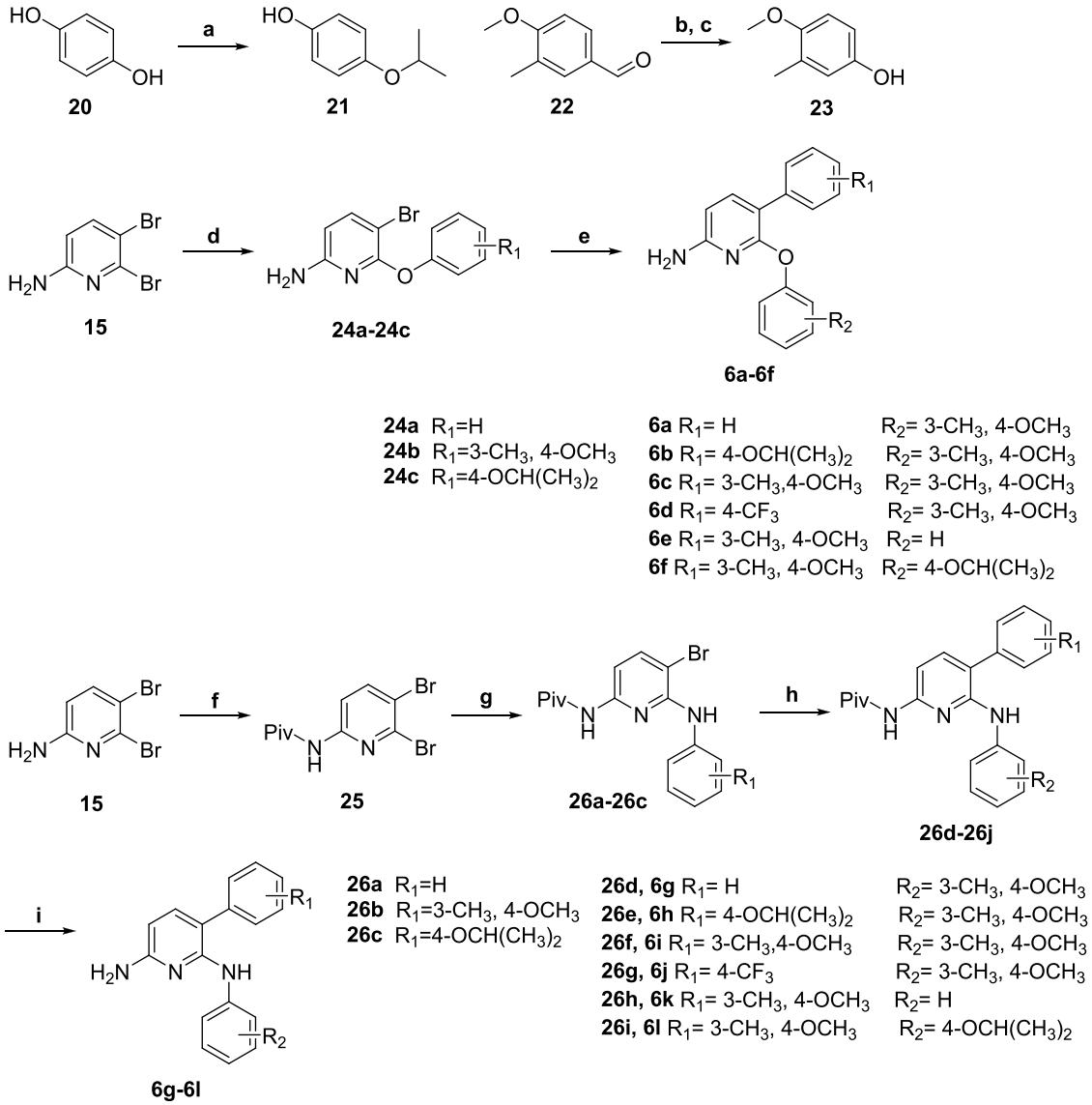

[c](a) 2-Iodine propane, KOH, EtOH; (b) *m*-3-chloroperoxybenzoic acid (CPBA), DCM; (c) 10% KOH, MeOH; (d) CuI, Cs_2CO_3, *N,N,N′,N′*-tetramethylethylenediamine (TMEDA), dimethylsulfoxide (DMSO); (e) (substituted phenyl)boronic Acid, $Pd(PPh_3)_4$, K_2CO_3, 1,4-dioxane/H_2O = 3:1; (f) TEA, 4-dimethylaminopyridine (DMAP), pivaloyl chloride, DCM; (g) substituted aniline, sodium *tert*-butoxide, $Pd(OAc)_2$, PPh_3, *o*-xylene; (h) 2-(substituted phenyl)-4,4,5,5-tetramethyl-1,3,2-dioxaborolane, $Pd(dppf)Cl_2$, Cs_2CO_3, DMF/H_2O = 6:1; (i) 3 N KOH, MeOH.

ethyl acetate in petroleum ether (1:10–1:4) to afford compounds **24a–c**.

4.1.6. General Procedure F. To a solution of compounds **24a–c** (2.6 mmol), (substituted phenyl)boronic acid (5.2 mmol), and K_2CO_3 (5.2 mmol) in the mixed solvent of 1,4-dioxane/H_2O = 90 mL:30 mL was added $Pd(PPh_3)_4$ (0.26 mmol) under a N_2 atmosphere. Then, the mixture was heated to 85 °C for 4 h. After completion of this reaction, it was cooled to room temperature. The mixture was poured into 100 mL of cold water and extracted with ethyl acetate. The combined organic layers were washed with brine, dried over Na_2SO_4, and then concentrated under vacuum. The residue was purified by silica gel chromatography using ethyl acetate in petroleum ether (1:5–1:2) to afford compounds **6a–f**.

4.1.7. General Procedure G. To a mixture of compound **25** (3 mmol), sodium *tert*-butoxide (7.64 mmol), $Pd(OAc)_2$ (0.45 mmol), and PPh_3 (0.6 mmol) in a sealed bottle was added substituted aniline dissolved in *o*-xylene (12 mL) under a N_2 atmosphere and then heated to 110 °C and reacted overnight. After completion of this reaction, the mixture was filtered. The filtrate was poured into 100 mL of water and extracted with ethyl acetate. The combined organic layers were washed with brine, dried over Na_2SO_4, and then concentrated under vacuum. The residue was purified by silica gel chromatography using ethyl acetate in petroleum ether (1:20–1:10) to afford compounds **26a–c**.

4.1.8. General Procedure H. To a solution of compounds **26a–c** (1.2 mmol), 2-(substituted phenyl)-4,4,5,5-tetramethyl-1,3,2-dioxaborolane (1.8 mmol), and Cs_2CO_3 (4.9 mmol) in the mixed solvent of DMF/H_2O = 24 mL:4 mL was added $Pd(dppf)Cl_2$ (0.12 mmol) under a N_2 atmosphere. Then, the mixture was heated to 85 °C for 3 h. After completion of this reaction, it was cooled to room temperature. The mixture was poured into 200 mL of cold water and extracted with ethyl acetate. The combined organic layers were washed with brine, dried over Na_2SO_4, and then concentrated under vacuum. The residue was purified by silica gel chromatography using ethyl acetate in petroleum ether (1:15–1:10) to afford compounds **26d–j**.

4.1.9. General Procedure I. To a solution of compounds **26d–j** (0.88 mmol) in methanol was added 5 mL of 3 N KOH and then

https://doi.org/10.1021/acs.jmedchem.1c00586
J. Med. Chem. 2021, 64, 8621–8643

Scheme 4. Synthetic Route for Target Compounds 7a–f[a]

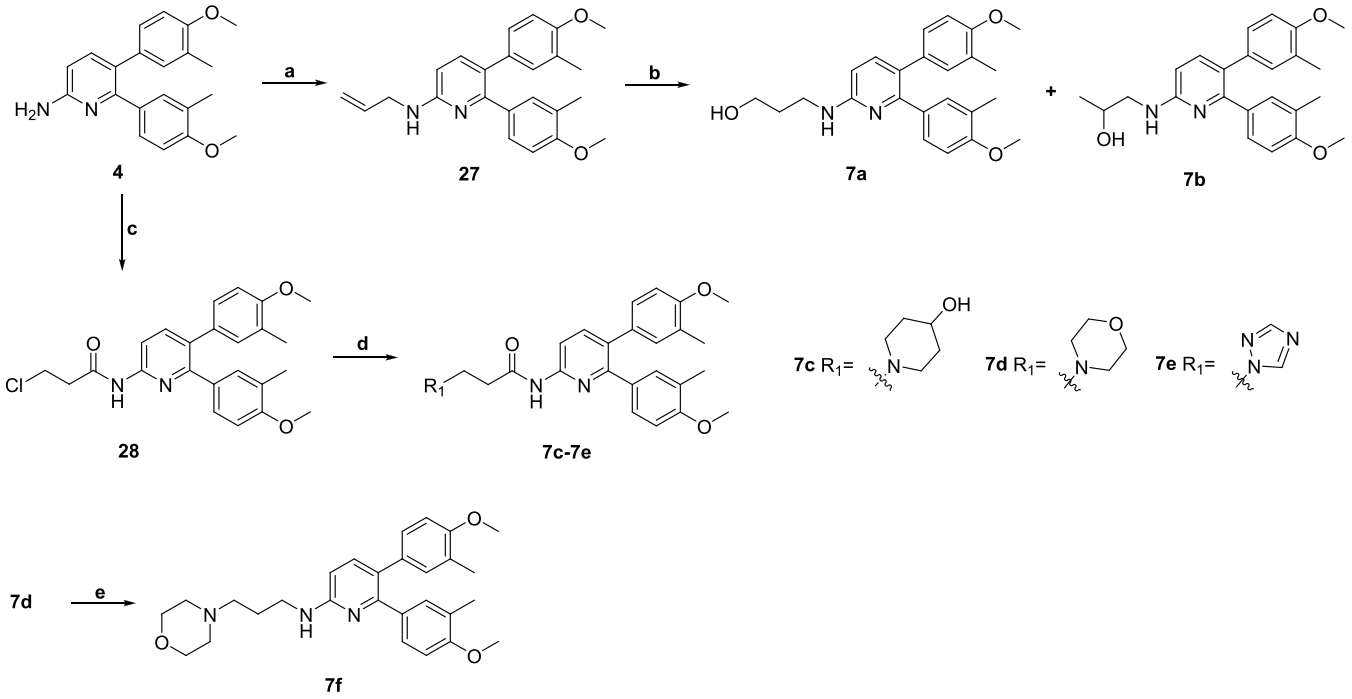

[a](a) Potassium *tert*-butoxide, allyl bromide, tetrahydrofuran (THF); (b) BH_3·THF, 30% H_2O_2, 3 N NaOH, THF; (c) 3-chloropropionyl chloride, TEA, DCM; (d) heterocycles, potassium iodide (KI), EtOH; (e) $LiAlH_4$, THF.

Scheme 5. Synthetic Route for Target Compounds 8a–i. (a) $SOCl_2$, DCM; (b) 2-Fluoro-5-nitroaniline, Pyridine, DCM; (c) Aliphatic Heterocycles, DIPEA, DMF; (d) Fe, NH_4Cl, EtOH/H_2O = 5:1

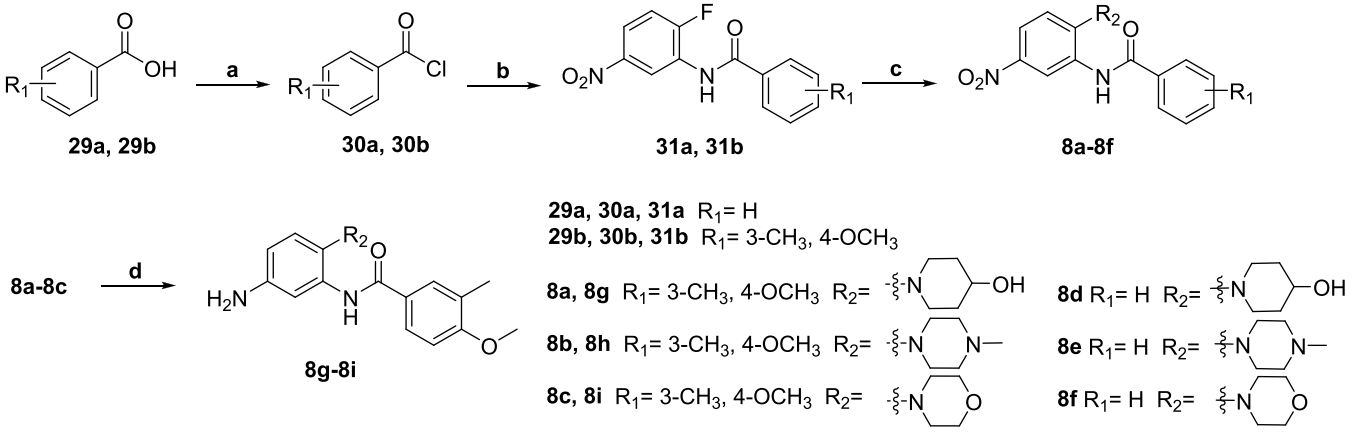

heated to reflux for 4 h. After completion of this reaction, the mixture was concentrated under vacuum. To the residue was added 50 mL of water and extracted with ethyl acetate. The combined organic layers were washed with brine, dried over Na_2SO_4, and then concentrated under vacuum. The residue was purified by silica gel chromatography using ethyl acetate in petroleum ether (1:20–1:10) to afford compounds **6g–l**.

4.1.10. General Procedure J. To a solution of compound **28** (0.47 mmol) and the indicated base (4.7 mmol) in 5 mL of ethanol was added KI (0.47 mmol) and then heated to reflux overnight. After completion of this reaction, it was cooled to room temperature. The mixture was poured into 100 mL of cold water and extracted with ethyl acetate. The combined organic layers were washed with brine, dried over Na_2SO_4, and then concentrated under vacuum. The residue was purified by silica gel chromatography using methanol in dichloromethane (1:30–1:20) to afford compounds **7c–e**.

4.1.11. General Procedure K. To a solution of compound **29a** or **29b** (16.4 mmol) in dichloromethane was added $SOCl_2$ (19.6 mmol) at 0 °C. The mixture was moved to room temperature and stirred for 3 h and then concentrated under vacuum to afford the acyl chloride **30a** or **30b**, which can be directly used in the next step.

To a solution of 2-fluoro-5-nitroaniline (6.3 mmol) in 10 mL of DCM was added **30a** or **30b** (8.1 mmol) and pyridine (8.1 mmol) dropwise. The mixture was stirred at room temperature overnight. After completion of the reaction, the mixture was concentrated under vacuum and a yellow solid can be precipitated out. The precipitate can be purified to afford compound **31a** or **31b** through stirring in the mixed solvent of ethyl acetate in petroleum ether (1:20) for 1 h.

4.1.12. General Procedure L. To a solution of compound **31a** or **31b** (1.64 mmol) in DMF (10 mL) were added 4-hydroxypiperidine (2.47 mmol) and DIPEA (3.26 mmol). The mixture was stirred at room temperature for 4 h. After completion of the reaction, the mixture was poured into 200 mL of water and extracted with ethyl acetate. The combined organic layers were washed with brine, dried over Na_2SO_4, and then concentrated under vacuum. The residue was purified by silica gel chromatography to afford compounds **8a–f**.

https://doi.org/10.1021/acs.jmedchem.1c00586
J. Med. Chem. 2021, 64, 8621–8643

4.1.13. General Procedure M. To a solution of compounds **8a−c** (0.4 mmol) in the mixed solvent of ethanol/H_2O = 10 mL:2 mL were added Fe (1.95 mmol) and NH_4Cl (0.8 mmol). The mixture was heated to reflux and mechanically stirred for 3 h. After completion of the reaction, the mixture was poured into 200 mL of water and extracted with ethyl acetate. The combined organic layers were washed with brine, dried over Na_2SO_4, and then concentrated under vacuum. The residue was purified by silica gel chromatography to afford compounds **8g−i**.

*4.1.14. 3-(2-Fluorophenyl)-4-(4-methoxy-3-methylphenyl)furan-2(5H)-one (**1a**).* General procedure A, yield: 62%; ^{1}H NMR (500 MHz, $CDCl_3$) δ 7.44−7.38 (m, 2H), 7.26−7.22 (m, 1H), 7.13 (t, J = 9.1 Hz, 2H), 7.07 (d, J = 1.9 Hz, 1H), 6.74 (d, J = 8.6 Hz, 1H), 5.25 (s, 2H), 3.83 (s, 3H), 2.12 (s, 3H). ^{13}C NMR (126 MHz, DMSO-d_6) δ 173.3, 161.0, 160.1, 159.6, 159.0, 132.2, 132.2, 131.5, 131.5, 129.8, 127.3, 126.6, 125.4, 125.4, 122.6, 119.7, 119.6, 117.4, 116.5, 116.3, 111.1, 71.3, 56.0, 16.4. ESI-MS: m/z = 299.2 $[M + H]^+$. High-resolution mass spectrometry (HRMS): calculated (M + H): 299.1083; found: 299.1079.

*4.1.15. 3-(2-Fluorophenyl)-4-(4-fluorophenyl)furan-2(5H)-one (**1b**).* General procedure A, yield: 43%; ^{1}H NMR (500 MHz, $CDCl_3$) δ 7.43 (dt, J = 7.2, 6.3 Hz, 2H), 7.32−7.28 (m, 2H), 7.27−7.24 (m, 1H), 7.14−7.09 (m, 1H), 7.06−7.02 (m, 2H), 5.25 (s, 2H). ^{13}C NMR (126 MHz, DMSO-d_6) δ 172.9, 164.8, 162.9, 160.9, 158.9, 158.9, 132.1, 132.1, 131.8, 131.8, 130.3, 130.2, 127.5, 127.4, 125.5, 125.5, 119.7, 118.9, 118.8, 116.8, 116.6, 116.6, 116.4, 71.5. ESI-MS: m/z = 273.2 $[M + H]^+$.

*4.1.16. 4-(4-Chlorophenyl)-3-(2-fluorophenyl)furan-2(5H)-one (**1c**).* General procedure A, yield: 66%; ^{1}H NMR (500 MHz, $CDCl_3$) δ 7.42 (m, 2H), 7.34−7.31 (m, 2H), 7.28−7.24 (m, 1H), 7.24−7.21 (m, 2H), 7.14−7.09 (m, 1H), 5.25 (s, 2H). ^{13}C NMR (126 MHz, DMSO-d_6) δ 172.7, 160.8, 158.8, 158.8, 136.2, 132.1, 132.1, 131.9, 131.8, 129.8, 129.6, 129.5, 125.5, 125.4, 120.4, 118.8, 118.7, 116.6, 116.5, 71.4. ESI-MS: m/z = 289.1 $[M + H]^+$.

*4.1.17. 3-(2-Fluorophenyl)-4-(4-isopropoxyphenyl)furan-2(5H)-one (**1d**).* General procedure A, yield: 71%; ^{1}H NMR (500 MHz, $CDCl_3$) δ 7.44−7.38 (m, 2H), 7.26−7.21 (m, 3H), 7.13 (dd, J = 13.8, 5.1 Hz, 1H), 6.82−6.78 (m, 2H), 5.25 (s, 2H), 4.56 (dt, J = 12.1, 6.1 Hz, 1H), 1.33 (s, 3H), 1.32 (s, 3H). ^{13}C NMR (126 MHz, DMSO-d_6) δ 173.3, 161.0, 160.3, 159.3, 159.0, 132.2, 132.2, 131.6, 131.5, 129.6, 125.5, 125.4, 122.6, 119.7, 119.6, 117.3, 116.6, 116.4, 116.1, 71.3, 70.0, 22.1. ESI-MS: m/z = 289.1 $[M + H]^+$.

*4.1.18. 3-(2-Fluorophenyl)-4-(3-methyl-4-propoxyphenyl)furan-2(5H)-one (**1e**).* General procedure A, yield: 31%; ^{1}H NMR (500 MHz, $CDCl_3$) δ 7.44−7.38 (m, 2H), 7.24 (td, J = 7.7, 1.1 Hz, 1H), 7.15−7.09 (m, 2H), 7.07 (d, J = 1.9 Hz, 1H), 6.71 (d, J = 8.6 Hz, 1H), 5.25 (s, 2H), 3.92 (t, J = 6.4 Hz, 2H), 2.13 (s, 3H), 1.85−1.78 (m, 2H), 1.04 (t, J = 7.4 Hz, 3H). ^{13}C NMR (126 MHz, DMSO-d_6) δ 173.3, 161.0, 159.6, 159.5, 159.0, 132.2, 132.2, 131.5, 131.5, 129.9, 127.3, 126.8, 125.4, 125.4, 122.4, 119.8, 119.7, 117.3, 116.5, 116.3, 111.8, 71.3, 69.6, 22.4, 16.4, 10.9. ESI-MS: m/z = 327.1 $[M + H]^+$.

*4.1.19. 3-(2-Fluorophenyl)-4-(3-methyl-4-(pentyloxy)phenyl)-furan-2(5H)-one (**1f**).* General procedure A, yield: 47%; ^{1}H NMR (500 MHz, $CDCl_3$) δ 7.43−7.38 (m, 2H), 7.24 (td, J = 7.6, 1.1 Hz, 1H), 7.15−7.05 (m, 3H), 6.71 (d, J = 8.6 Hz, 1H), 5.25 (s, 2H), 3.95 (t, J = 6.4 Hz, 2H), 2.12 (s, 3H), 1.82−1.76 (m, 2H), 1.46−1.35 (m, 4H), 0.92 (t, J = 7.2 Hz, 3H). ^{13}C NMR (126 MHz, DMSO-d_6) δ 173.3, 161.00, 159.6, 159.5, 159.0, 132.2, 132.2, 131.5, 131.5, 129.9, 127.3, 126.7, 125.4, 125.4, 122.4, 119.8, 119.6, 117.3, 116.5, 116.3, 111.8, 71.3, 68.2, 28.7, 28.2, 22.3, 16.4, 14.4. ESI-MS: m/z = 355.2 $[M + H]^+$.

*4.1.20. 4-(2-Fluorophenyl)-3-(4-methoxyphenyl)furan-2(5H)-one (**2a**).* General procedure A, yield: 13%; ^{1}H NMR (500 MHz, $CDCl_3$) δ 7.44−7.39 (m, 3H), 7.26 (dd, J = 7.5, 1.6 Hz, 1H), 7.18 (dd, J = 10.7, 8.5 Hz, 1H), 7.11 (dd, J = 11.1, 4.1 Hz, 1H), 6.91−6.87 (m, 2H), 5.20 (d, J = 1.3 Hz, 2H), 3.84 (s, 3H). ^{13}C NMR (126 MHz, DMSO-d_6) δ 172.9, 160.2, 160.0, 158.3, 151.9, 132.8, 132.7, 130.5, 130.5, 130.1, 126.9, 125.5, 125.5, 122.8, 119.8, 119.7, 117.0, 116.9, 114.4, 71.5, 71.5, 55.6. ESI-MS: m/z = 285.1 $[M + H]^+$.

*4.1.21. 4-(4-(2-Fluorophenyl)-2-oxo-2,5-dihydrofuran-3-yl)-phenyl Acetate (**2b**).* General procedure A, yield: 30%; ^{1}H NMR (500 MHz, $CDCl_3$) δ 7.47−7.44 (m, 2H), 7.40 (m, 1H), 7.22 (m, 1H), 7.18−7.14 (m, 1H), 7.12−7.07 (m, 3H), 5.20 (d, J = 2.3 Hz, 2H), 3.30 (s, 3H). ESI-MS: m/z = 314.1 $[M + H]^+$.

*4.1.22. 4-(2-Fluorophenyl)-3-(4-fluorophenyl)furan-2(5H)-one (**2c**).* General procedure A, yield: 35%; ^{1}H NMR (500 MHz, $CDCl_3$) δ 7.44−7.39 (m, 3H), 7.22−7.14 (m, 2H), 7.10 (m, 1H), 7.04 (m, 2H), 5.19 (d, J = 2.2 Hz, 2H). ESI-MS: m/z = 274.2 $[M + H]^+$.

*4.1.23.10. 4-(2-Fluorophenyl)-3-(4-(trifluoromethyl)phenyl)-furan-2(5H)-one (**2d**).* General procedure A, yield: 28%; ^{1}H NMR (500 MHz, $CDCl_3$) δ 7.58 (m, 4H), 7.47−7.42 (m, 1H), 7.20−7.15 (m, 2H), 7.14−7.10 (m, 1H), 5.24 (d, J = 2.2 Hz, 2H). ESI-MS: m/z = 322.0 $[M + H]^+$.

*4.1.24. 4-(2-Fluorophenyl)-3-(1H-indol-3-yl)furan-2(5H)-one (**2e**).* General procedure A, yield: 21%; ^{1}H NMR (500 MHz, DMSO-d_6) δ 12.53 (s, 1H), 7.71 (m, 1H), 7.48−7.43 (m, 2H), 7.39 (d, J = 8.1 Hz, 1H), 7.22 (m, 1H), 7.16 (m, 1H), 7.04−7.00 (m, 1H), 6.73−6.68 (m, 1H), 6.59 (m, 1H), 5.34 (s, 2H). ^{13}C NMR (126 MHz, DMSO-d_6) δ 173.6, 160.7, 158.7, 147.5, 136.6, 132.4, 132.3, 130.4, 130.4, 127.7, 125.2, 125.1, 125.0, 122.4, 121.9, 120.9, 120.8, 120.00, 119.7, 116.8, 116.6, 112.4, 105.1, 71.7, 71.6. ESI-MS: m/z = 294.2 $[M + H]^+$.

*4.1.25. 3-(1-Ethyl-1H-indol-3-yl)-4-(2-fluorophenyl)furan-2(5H)-one (**2f**).* General procedure A, yield: 4%; ^{1}H NMR (500 MHz, $CDCl_3$) δ 7.83 (s, 1H), 7.34 (t, J = 7.8 Hz, 2H), 7.31 (d, J = 6.2 Hz, 1H), 7.29 (s, 1H), 7.15 (dd, J = 14.9, 7.6 Hz, 2H), 6.95 (t, J = 7.6 Hz, 1H), 6.82 (t, J = 7.5 Hz, 1H), 6.66 (d, J = 8.2 Hz, 1H), 5.29 (s, 2H), 4.24 (q, J = 7.3 Hz, 2H), 1.54 (m, 3H). ^{13}C NMR (126 MHz, DMSO-d_6) δ 173.5, 160.7, 158.7, 147.4, 136.1, 132.4, 132.3, 130.3, 130.3, 130.1, 125.6, 125.2, 125.2, 122.0, 122.0, 120.9, 120.8, 120.3, 119.8, 116.8, 116.6, 110.8, 104.5, 71.7, 71.6, 41.1, 15.8. ESI-MS: m/z = 323.2 $[M + H]^+$.

*4.1.26. 4-(2-Fluorophenyl)-3-(naphthalen-1-yl)furan-2(5H)-one (**2g**).* General procedure A, yield: 48%; ^{1}H NMR (500 MHz, $CDCl_3$) δ 7.89 (m, 2H), 7.65 (d, J = 8.4 Hz, 1H), 7.53−7.46 (m, 2H), 7.44−7.38 (m, 2H), 7.26−7.23 (m, 1H), 7.08 (m, 1H), 6.91 (m, 1H), 6.79−6.75 (m, 1H), 5.53−5.41 (m, 2H). ^{13}C NMR (126 MHz, DMSO-d_6) δ 173.1, 160.7, 158.7, 155.8, 133.7, 133.1, 133.1, 131.1, 130.1, 130.1, 129.5, 129.1, 128.9, 128.1, 127.4, 126.9, 126.7, 126.1, 125.4, 125.2, 125.2, 119.1, 119.0, 117.0, 116.8, 72.2, 72.2. ESI-MS: m/z = 305.2 $[M + H]^+$.

*4.1.27. 3,4-Bis(2-fluorophenyl)-1H-pyrrole-2,5-dione (**3a**).* General procedure B, yield: 52%; ^{1}H NMR (500 MHz, DMSO-d_6) δ 11.48 (s, 1H), 7.51−7.46 (m, 2H), 7.41 (td, J = 7.5, 1.7 Hz, 2H), 7.26 (td, J = 7.6, 1.0 Hz, 2H), 7.22 (dd, J = 10.4, 8.4 Hz, 2H). ^{13}C NMR (126 MHz, DMSO-d_6) δ 170.8, 160.8, 158.8, 135.7, 132.6, 132.5, 131.9, 131.9, 124.9, 124.8, 117.5, 117.3, 116.4, 116.2. ESI-MS: m/z = 284.0 $[M - H]^-$.

*4.1.28. 3-(2-Fluorophenyl)-4-(4-methoxyphenyl)-1H-pyrrole-2,5-dione (**3b**).* General procedure B, yield: 25%; ^{1}H NMR (500 MHz, $CDCl_3$) δ 7.60 (s, 1H), 7.46 (m, 4H), 7.24 (s, 1H), 7.12 (d, J = 8.4 Hz, 1H), 6.85 (d, J = 7.6 Hz, 2H), 3.82 (s, 3H). ^{13}C NMR (126 MHz, DMSO-d_6) δ 172.1, 171.4, 161.1, 160.8, 158.8, 138.8, 132.3, 132.3, 132.2, 132.1, 131.3, 130.3, 125.2, 125.1, 121.6, 117.9, 117.8, 116.5, 116.4, 114.5, 55.7. ESI-MS: m/z = 296.1 $[M - H]^-$.

*4.1.29. 3-(2-Fluorophenyl)-4-(4-methoxy-3-methylphenyl)-1H-pyrrole-2,5-dione (**3c**).* General procedure B, yield: 52%; ^{1}H NMR (500 MHz, $CDCl_3$) δ 7.55 (s, 1H), 7.47−7.36 (m, 3H), 7.33 (s, 1H), 7.25−7.21 (m, 1H), 7.11 (dt, J = 19.0, 9.5 Hz, 1H), 6.76 (d, J = 8.6 Hz, 1H), 3.83 (s, 3H), 2.12 (s, 3H). ^{13}C NMR (126 MHz, DMSO-d_6) δ 172.1, 171.4, 160.8, 159.3, 158.8, 138.9, 132.3, 132.3, 132.1, 132.1, 131.7, 130.2, 129.2, 126.0, 125.1, 125.1, 121.9, 116.5, 116.3, 110.8, 71.3, 55.9, 16.5. ESI-MS: m/z = 310.1 $[M - H]^-$.

*4.1.30. 5,6-Dibromopyridin-2-amine (**15**).* To a solution of 6-bromopyridin-2-amine (28.7 mmol) in 100 mL of dry dichloromethane was added NBS (28.9 mmol) slowly. The mixture was stirred at room temperature for 6 h. After completion of the reaction, the mixture was poured into 100 mL of water and extracted with dichloromethane. The combined organic layers were washed with brine, dried over Na_2SO_4, and then concentrated under vacuum. The

https://doi.org/10.1021/acs.jmedchem.1c00586
J. Med. Chem. 2021, 64, 8621−8643

residue was purified by silica gel chromatography using ethyl acetate in petroleum ether (1:10−1:5) to afford the compound, yield: 73.9%; ^{1}H NMR (400 MHz, $CDCl_3$) δ 7.60 (d, J = 8.5 Hz, 1H), 6.42 (d, J = 8.5 Hz, 1H), 4.48 (s, 2H). ESI-MS: m/z = 250.8 $[M + H]^+$.

*4.1.31. 5-Bromo-6-phenylpyridin-2-amine (**16a**).* General procedure C, yield: 79.2%; ^{1}H NMR (400 MHz, $CDCl_3$) δ 7.69−7.56 (m, 3H), 7.47−7.34 (m, 3H), 6.37 (d, J = 8.6 Hz, 1H), 4.59 (s, 2H). ESI-MS: m/z = 249.0 $[M + H]^+$.

*4.1.32. 5-Bromo-6-(4-isopropoxyphenyl)pyridin-2-amine (**16b**).* General procedure C, yield: 82.5%; ^{1}H NMR (400 MHz, $CDCl_3$) δ 7.77−7.73 (m, 1H), 7.68−7.52 (m, 2H), 7.03−6.89 (m, 2H), 6.65 (d, J = 9.0 Hz, 1H), 6.54 (s, 1H), 4.62 (hept, J = 6.1 Hz, 1H), 1.36 (d, J = 6.0 Hz, 6H). ESI-MS: m/z = 307.0 $[M + H]^+$.

*4.1.33. 5-Bromo-6-(4-methoxy-3-methylphenyl)pyridin-2-amine (**16c**).* General procedure C, yield: 83.7%; ^{1}H NMR (400 MHz, $CDCl_3$) δ 7.69 (d, J = 8.6 Hz, 1H), 7.53 (dd, J = 8.4, 2.3 Hz, 1H), 7.47 (d, J = 2.3 Hz, 1H), 6.92 (d, J = 8.4 Hz, 1H), 6.40 (d, J = 8.6 Hz, 1H), 4.71 (s, 2H), 3.91 (s, 3H), 2.31 (s, 3H). ESI-MS: m/z = 292.8 $[M + H]^+$.

*4.1.34. 5,6-Bis(4-methoxy-3-methylphenyl)pyridin-2-amine (**4**).* General procedure D, yield: 50%; ^{1}H NMR (400 MHz, DMSO-d_6) δ 7.34 (d, J = 8.3 Hz, 1H), 7.22 (d, J = 1.6 Hz, 1H), 6.93 (dd, J = 6.7, 3.7 Hz, 2H), 6.81 (d, J = 2.2 Hz, 2H), 6.73 (d, J = 8.5 Hz, 1H), 6.46 (d, J = 8.3 Hz, 1H), 5.96 (s, 2H), 3.76 (s, 3H), 3.75 (s, 3H), 2.09 (s, 6H). ^{13}C NMR (126 MHz, DMSO-d_6) δ 158.6, 156.9, 156.1, 154.0, 140.4, 133.3, 133.3, 132.2, 131.6, 128.8, 128.3, 125.5, 124.7, 123.7, 110.4, 109.4, 106.7, 55.6, 16.6. ESI-MS: m/z = 335.3 $[M + H]^+$. HRMS: calculated (M + H): 335.1760; found: 335.1754.

*4.1.35. 5-(4-Methoxy-3-methylphenyl)-6-phenylpyridin-2-amine (**5a**).* General procedure D, yield: 94.1%; melting point: 162−164 °C; retention time: 8.996 min; purity: 99.09%; ^{1}H NMR (400 MHz, $CDCl_3$) δ 7.53 (dd, J = 8.3, 1.6 Hz, 1H), 7.39 (dh, J = 7.9, 2.4, 1.9 Hz, 2H), 7.27 (dt, J = 6.0, 1.9 Hz, 3H), 6.96 (d, J = 2.2 Hz, 1H), 6.88 (dd, J = 8.5, 2.2 Hz, 1H), 6.69 (dd, J = 8.4, 1.5 Hz, 1H), 6.56 (dd, J = 8.3, 1.7 Hz, 1H), 4.67 (s, 2H), 3.83 (s, 3H), 2.17 (s, 3H). ^{13}C NMR (100 MHz, $CDCl_3$) δ 156.8, 156.5, 154.9, 140.7, 140.6, 132.2, 131.9, 129.8, 128.1, 127.8, 127.4, 126.4, 126.3, 109.6, 107.3, 55.3, 16.2. ESI-MS: m/z = 291.0 $[M + H]^+$. HRMS: calculated (M + H): 291.1497; found: 291.1503.

*4.1.36. 6-(4-Isopropoxyphenyl)-5-(4-methoxy-3-methylphenyl)-pyridin-2-amine (**5b**).* General procedure D, yield: 80.2%; melting point: 137−140 °C; retention time: 11.505 min; purity: 99.34%; ^{1}H NMR (400 MHz, $CDCl_3$) δ 7.45 (d, J = 8.3 Hz, 1H), 7.28−7.24 (m, 2H), 6.95−6.89 (m, 1H), 6.86 (dd, J = 8.3, 2.3 Hz, 1H), 6.79−6.70 (m, 2H), 6.67 (d, J = 8.4 Hz, 1H), 6.48 (d, J = 8.3 Hz, 1H), 4.61 (s, 2H), 4.51 (h, J = 6.1 Hz, 1H), 3.79 (s, 3H), 2.13 (s, 3H), 1.30 (d, J = 6.1 Hz, 6H). ^{13}C NMR (100 MHz, $CDCl_3$) δ 157.4, 156.7, 156.4, 154.5, 140.8, 132.8, 132.4, 131.8, 131.0 × 2, 128.0, 126.2, 126.1, 115.4 × 2, 109.7, 106.8, 69.9, 55.3, 22.0 × 2, 16.1. ESI-MS: m/z = 349.0 $[M + H]^+$. HRMS: calculated (M + H): 349.1916; found: 349.1929.

*4.1.37. 6-(4-Methoxy-3-methylphenyl)-5-phenylpyridin-2-amine (**5d**).* General procedure D, yield: 89.2%; melting point: 187−190 °C; retention time: 9.264 min; purity: 98.40%; ^{1}H NMR (400 MHz, $CDCl_3$) δ 7.51 (d, J = 8.3 Hz, 1H), 7.31−7.23 (m, 4H), 7.21−7.15 (m, 2H), 7.07 (dd, J = 8.4, 2.3 Hz, 1H), 6.66 (d, J = 8.5 Hz, 1H), 6.54 (d, J = 8.3 Hz, 1H), 4.63 (s, 2H), 3.82 (s, 3H), 2.18 (s, 3H). ^{13}C NMR (100 MHz, $CDCl_3$) δ 157.4, 157.1, 155.2, 140.8, 140.6, 132.4, 132.1, 129.6 × 2, 128.6, 128.1 × 2, 126.3, 126.1, 125.9, 117.2, 109.1, 106.6, 77.4, 77.3, 77.1, 76.7, 55.3, 16.2. ESI-MS: m/z = 291.0 $[M + H]^+$. HRMS: calculated (M + H): 291.1497; found: 291.1503.

*4.1.38. 5-(4-Isopropoxyphenyl)-6-(4-methoxy-3-methylphenyl)-pyridin-2-amine (**5e**).* General procedure D, yield: 81.6%; melting point: 157−159 °C; retention time: 11.516 min; purity: 98.86%; ^{1}H NMR (400 MHz, $CDCl_3$) δ 7.50 (d, J = 8.3 Hz, 1H), 7.27 (d, J = 2.3 Hz, 1H), 7.10 (dd, J = 8.4, 2.2 Hz, 1H), 7.07 (d, J = 8.2 Hz, 2H), 6.81 (d, J = 8.3 Hz, 2H), 6.68 (d, J = 8.4 Hz, 1H), 6.53 (d, J = 8.3 Hz, 1H), 4.62 (s, 2H), 4.56 (p, J = 6.0 Hz, 1H), 3.83 (s, 3H), 2.19 (s, 3H), 1.37 (d, J = 6.0 Hz, 6H). ^{13}C NMR (100 MHz, $CDCl_3$) δ 156.8, 156.4, 154.9, 140.6, 133.0, 132.5, 132.1, 130.6 × 2, 128.6, 126.0, 125.9, 115.7 × 2, 109.2, 106.7, 70.0, 55.3, 22.1 × 2, 16.2. ESI-MS: m/z = 348.9 $[M + H]^+$. HRMS: calculated (M + H): 349.1916; found: 349.1925.

*4.1.39. 6-(4-Methoxy-3-methylphenyl)-5-(4-(trifluoromethyl)-phenyl)pyridin-2-amine (**5f**).* General procedure D, yield: 82.1%; melting point: 192−195 °C; retention time: 10.802 min; purity: 99.32%; ^{1}H NMR (400 MHz, $CDCl_3$) δ 7.51 (t, J = 8.6 Hz, 3H), 7.27 (s, 2H), 7.25−7.22 (m, 1H), 7.02 (dd, J = 8.4, 2.2 Hz, 1H), 6.67 (d, J = 8.4 Hz, 1H), 6.56 (d, J = 8.3 Hz, 1H), 4.72 (s, 2H), 3.83 (s, 3H), 2.18 (s, 3H). ^{13}C NMR (100 MHz, $CDCl_3$) δ 157.7, 157.5, 155.5, 144.6, 140.4, 132.0, 131.8, 129.8 × 2, 128.6, 128.4, 126.3, 125.0 × 2, 124.7, 109.3, 106.7, 55.3, 16.1. ESI-MS: m/z = 358.9 $[M + H]^+$. HRMS: calculated (M + H): 359.1371; found: 359.1378.

*4.1.40. 5-Bromo-6-chloropyridin-2-amine (**18**).* To a solution of 6-chloropyridin-2-amine (15.6 mmol) in 30 mL of dry dichloromethane was added NBS (17.1 mmol) slowly. The mixture was stirred at room temperature for 8 h. After completion of the reaction, the mixture was poured into 100 mL of water and extracted with dichloromethane. The combined organic layers were washed with brine, dried over Na_2SO_4, and then concentrated under vacuum. The residue was purified by silica gel chromatography using ethyl acetate in petroleum ether (1:10−1:5) to afford the compound, yield: 53.5%; ^{1}H NMR (400 MHz, $CDCl_3$) δ 7.27 (d, J = 8.5 Hz, 1H), 6.01 (d, J = 8.5 Hz, 1H), 3.95 (s, 2H). ESI-MS: m/z = 206.9 $[M + H]^+$.

*4.1.41. 6-Chloro-5-(4-methoxy-3-methylphenyl) pyridin-2-amine (**19**).* To the mixture of compound **14** (2.43 mmol), 2-(4-methoxy-3-methylphenyl)-4,4,5,5-tetramethyl-1,3,2-dioxaborolane (2.65 mmol), and K_2CO_3 (6 mmol) in the mixed solvent of toluene/ethanol = 5 mL:3 mL was added $Pd(PPh_3)_4$ (0.24 mmol) under a nitrogen atmosphere. The reaction mixture was heated to 80 °C for 8 h. After the solvent was removed under vacuum, to the residue was added water and extracted with ethyl acetate. The combined organic layers were washed with brine, dried over Na_2SO_4, and concentrated to afford the crude product, and then, recrystallization using methanol was performed to afford the white powder; yield: 67.7%; ^{1}H NMR (400 MHz, $CDCl_3$) δ 7.41 (d, J = 8.2 Hz, 1H), 7.22 (dd, J = 8.3, 2.4 Hz, 1H), 7.20−7.15 (m, 1H), 6.86 (d, J = 8.4 Hz, 1H), 6.47 (d, J = 8.2 Hz, 1H), 4.57 (s, 2H), 3.87 (s, 3H), 2.26 (s, 3H). ESI-MS: m/z = 249.0 $[M + H]^+$.

*4.1.42. 5-(4-Methoxy-3-methylphenyl)-6-(4-(trifluoromethyl)-phenyl)pyridin-2-amine (**5c**).* To a solution of compound **15** (0.605 mmol), 4,4,5,5-tetramethyl-2-(4-(trifluoromethyl)phenyl)-1,3,2-dioxaborolane (1.13 mmol), Cs_2CO_3 (3.02 mmol), and XPhos (0.072 mmol) in 4 mL of n-butyl alcohol was added $Pd(OAc)_2$ (0.036 mmol) under a N_2 atmosphere. The mixture was heated to 100 °C and stirred overnight. After completion of the reaction, the mixture was poured into 100 mL of water and extracted with ethyl acetate. The combined organic layers were washed with brine, dried over Na_2SO_4, and then concentrated under vacuum. The residue was purified by silica gel chromatography using ethyl acetate in petroleum ether (1:8−1:2) to afford the compound, yield: 11.6%; melting point: 130−132 °C; retention time: 10.067 min; purity: 99.70%; ^{1}H NMR (400 MHz, $CDCl_3$) δ 7.56−7.43 (m, 5H), 6.93−6.87 (m, 1H), 6.81 (dd, J = 8.4, 2.3 Hz, 1H), 6.67 (d, J = 8.4 Hz, 1H), 6.56 (d, J = 8.3 Hz, 1H), 4.58 (s, 2H), 3.80 (s, 3H), 2.14 (s, 3H). ^{13}C NMR (100 MHz, $CDCl_3$) δ 157.0, 156.7, 153.4, 144.4, 140.8, 131.8, 131.5, 130.1 × 2, 128.1, 126.7, 126.6, 124.7 × 2, 109.8, 107.9, 55.3, 16.1. ESI-MS: m/z = 359.2 $[M + H]^+$. HRMS: calculated (M + H): 359.1371; found: 359.1381.

*4.1.43. 5-Bromo-6-phenoxypyridin-2-amine (**24a**).* General procedure E, yield: 79.7%; ^{1}H NMR (400 MHz, $CDCl_3$) δ 7.60 (d, J = 8.3 Hz, 1H), 7.42−7.30 (m, 2H), 7.21−7.14 (m, 1H), 7.13−7.07 (m, 2H), 6.12 (d, J = 8.3 Hz, 1H). ESI-MS: m/z = 365.0 $[M + H]^+$.

*4.1.44. 5-Bromo-6-(4-methoxy-3-methylphenoxy)pyridin-2-amine (**24b**).* General procedure E, yield: 81.1%. ESI-MS: m/z = 309.0 $[M + H]^+$.

*4.1.45. 5-Bromo-6-(4-isopropoxyphenoxy)pyridin-2-amine (**24c**).* General procedure E, yield: 83.5%. ESI-MS: m/z = 323 $[M + H]^+$.

*4.1.46. 6-(4-Methoxy-3-methylphenoxy)-5-phenylpyridin-2-amine (**6a**).* General procedure F, yield: 88.4%; melting point: 127−129 °C; retention time: 18.213 min; purity: 100.00%; ^{1}H NMR

https://doi.org/10.1021/acs.jmedchem.1c00586
J. Med. Chem. 2021, 64, 8621−8643

(400 MHz, $CDCl_3$) δ 7.70−7.57 (m, 3H), 7.44 (t, J = 7.6 Hz, 2H), 7.37−7.31 (m, 1H), 6.96 (d, J = 8.1 Hz, 2H), 6.84 (d, J = 8.3 Hz, 1H), 6.30 (d, J = 8.0 Hz, 1H), 4.26 (s, 2H), 3.87 (s, 3H), 2.27 (s, 3H). ^{13}C NMR (100 MHz, $CDCl_3$) δ 159.2, 156.6, 154.1, 147.9, 141.5, 137.1, 128.8 × 2, 128.2 × 2, 127.5, 126.5, 123.4, 118.6, 114.6, 110.4, 102.7, 55.7, 16.3. ESI-MS: m/z = 307.0 $[M + H]^+$. HRMS: calculated (M + H): 307.1447; found: 307.1453.

*4.1.47. 5-(4-Isopropoxyphenyl)-6-(4-methoxy-3-methylphenoxy)pyridin-2-amine (**6b**).* General procedure F, yield: 90.9%; melting point: 171−174 °C; retention time: 19.192 min; purity: 99.57%; ^{1}H NMR (400 MHz, $CDCl_3$) δ 7.56 (t, J = 7.9 Hz, 3H), 6.95 (h, J = 3.1 Hz, 4H), 6.83 (d, J = 8.3 Hz, 1H), 6.28 (d, J = 8.0 Hz, 1H), 4.61 (hept, J = 6.1 Hz, 1H), 4.24 (s, 2H), 3.86 (s, 3H), 2.26 (s, 3H), 1.40 (d, J = 6.2 Hz, 6H). ^{13}C NMR (100 MHz, $CDCl_3$) δ 159.0, 156.8, 156.1, 154.1, 148.1, 141.3, 129.8 × 2, 129.2, 127.5, 123.3, 118.5, 115.6 × 2, 114.5, 110.4, 102.8, 69.9, 55.7, 22.2 × 2, 16.3. ESI-MS: m/z = 365.0 $[M + H]^+$. HRMS: calculated (M + H): 365.1865; found: 365.1868.

*4.1.48. 6-(4-Methoxy-3-methylphenoxy)-5-(4-methoxy-3-methylphenyl)pyridin-2-amine (**6c**).* General procedure F, yield: 80.5%; melting point: 130−132 °C; retention time: 16.616 min; purity: 99.68%; ^{1}H NMR (400 MHz, $CDCl_3$) δ 7.56 (d, J = 8.0 Hz, 1H), 7.46 (dd, J = 8.3, 2.3 Hz, 1H), 7.40 (d, J = 2.3 Hz, 1H), 6.98−6.87 (m, 3H), 6.83 (d, J = 8.3 Hz, 1H), 6.28 (d, J = 8.0 Hz, 1H), 4.77−3.91 (m, 1H), 3.88 (d, J = 11.0 Hz, 6H), 2.28 (d, J = 18.0 Hz, 6H). ^{13}C NMR (100 MHz, $CDCl_3$) δ 159.1, 156.7, 156.1, 154.1, 148.1, 141.3, 131.1, 129.1, 127.5, 127.2, 126.3, 123.3, 118.6, 114.7, 110.4, 109.8, 102.7, 55.7, 55.4, 16.3 × 2. ESI-MS: m/z = 351.0 $[M + H]^+$. HRMS: calculated (M + H): 351.1709; found: 351.1713.

*4.1.49. 6-(4-Methoxy-3-methylphenoxy)-5-(4-(trifluoromethyl)-phenyl)pyridin-2-amine (**6d**).* General procedure F, yield: 61.8%; melting point: 146−149 °C; retention time: 15.461 min; purity: 100.00%; ^{1}H NMR (400 MHz, $CDCl_3$) δ 7.76 (d, J = 8.7 Hz, 2H), 7.68 (d, J = 8.2 Hz, 2H), 7.60 (dd, J = 8.1, 0.7 Hz, 1H), 6.98−6.90 (m, 2H), 6.88−6.80 (m, 1H), 6.30 (dd, J = 8.1, 0.7 Hz, 1H), 4.21 (d, J = 127.2 Hz, 2H), 3.87 (s, 3H), 2.26 (s, 3H). ^{13}C NMR (100 MHz, $CDCl_3$) δ 159.3, 157.1, 154.4, 147.4, 141.4, 140.8, 129.0 × 2, 127.7, 125.0 × 2, 123.4, 118.7, 112.8, 110.4, 102.7, 55.7, 16.3. ESI-MS: m/z = 375.1 $[M + H]^+$. HRMS: calculated (M + H): 375.1320; found: 375.1323.

*4.1.50. 5-(4-Methoxy-3-methylphenyl)-6-phenoxypyridin-2-amine (**6e**).* General procedure F, yield: 79.8%; melting point: 155−156 °C; retention time: 14.570 min; purity: 100.00%; ^{1}H NMR (400 MHz, $CDCl_3$) δ 7.59 (d, J = 8.0 Hz, 1H), 7.44 (dd, J = 8.4, 2.3 Hz, 1H), 7.42−7.34 (m, 3H), 7.21−7.10 (m, 3H), 6.89 (d, J = 8.4 Hz, 1H), 6.32 (d, J = 8.1 Hz, 1H), 4.07 (s, 2H), 3.89 (s, 3H), 2.30 (s, 3H). ^{13}C NMR (100 MHz, $CDCl_3$) δ 158.4, 156.8, 156.2, 155.4, 141.5, 131.1, 129.2 × 2, 128.9, 127.2, 126.3, 123.4, 120.5 × 2, 115.2, 109.8, 103.4, 55.4, 16.3. ESI-MS: m/z = 307.1 $[M + H]^+$. HRMS: calculated (M + H): 307.1447; found: 307.1452.

*4.1.51. 6-(4-Isopropoxyphenoxy)-5-(4-methoxy-3-methylphenyl)pyridin-2-amine (**6f**).* General procedure F, yield: 83.5%; melting point: 144−147 °C; retention time: 17.526 min; purity: 100.00%; ^{1}H NMR (400 MHz, $CDCl_3$) δ 7.56 (d, J = 8.0 Hz, 1H), 7.49−7.37 (m, 2H), 7.05 (d, J = 8.7 Hz, 2H), 6.90 (dd, J = 8.9, 3.6 Hz, 3H), 6.28 (d, J = 8.0 Hz, 1H), 4.53 (hept, J = 6.1 Hz, 1H), 4.45−4.22 (m, 2H), 3.89 (s, 3H), 2.30 (s, 3H), 1.38 (d, J = 6.0 Hz, 6H). ^{13}C NMR (100 MHz, $CDCl_3$) δ 159.0, 156.7, 156.1, 154.1, 148.5, 141.3, 131.1, 129.1, 127.2, 126.3, 121.8 × 2, 116.6 × 2, 114.7, 109.8, 102.7, 70.6, 55.4, 22.2 × 2, 16.3. ESI-MS: m/z = 365.1 $[M + H]^+$. HRMS: calculated (M + H): 365.1865; found: 365.1871.

*4.1.52. N-(5,6-Dibromopyridin-2-yl)pivalamide (**25**).* To a solution of compound **11** (23.8 mmol), TEA (35.7 mmol), and DMAP (2.38 mmol) dissolved in anhydrous DCM was added pivaloyl chloride (35.7 mmol) at 0 °C. The mixture was moved to room temperature and stirred overnight. After completion of this reaction, the mixture was concentrated under vacuum. The residue was dissolved in DCM, washed with brine, dried over Na_2SO_4, and then concentrated under vacuum. The residue was purified by silica gel chromatography using ethyl acetate in petroleum ether (1:20) to afford the compound, yield: 88.6%; ^{1}H NMR (400 MHz, $CDCl_3$) δ 8.18 (d, J = 8.6 Hz, 1H), 8.03 (s, 1H), 7.88 (d, J = 8.6 Hz, 1H), 1.35 (s, 9H). ESI-MS: m/z = 334.9 $[M + H]^+$.

*4.1.53. N-(5-Bromo-6-(phenylamino)pyridin-2-yl)pivalamide (**26a**).* General procedure G, yield: 60.1%; ^{1}H NMR (400 MHz, $CDCl_3$) δ 7.90 (s, 1H), 7.77 (d, J = 8.5 Hz, 1H), 7.67 (d, J = 8.5 Hz, 1H), 7.61−7.54 (m, 2H), 7.45−7.36 (m, 2H), 7.13 (tt, J = 7.3, 1.2 Hz, 1H), 6.99 (s, 1H), 1.36 (s, 9H). ESI-MS: m/z = 348.1 $[M + H]^+$.

*4.1.54. N-(5-Bromo-6-((4-methoxy-3-methylphenyl)amino)-pyridin-2-yl)pivalamide (**26b**).* General procedure G, yield: 50.6%; ^{1}H NMR (400 MHz, $CDCl_3$) δ 7.69 (d, J = 8.5 Hz, 1H), 7.58 (d, J = 8.5 Hz, 1H), 7.32 (dd, J = 8.7, 2.7 Hz, 1H), 7.21 (d, J = 2.7 Hz, 1H), 6.83 (d, J = 8.7 Hz, 1H), 6.76 (s, 1H), 3.85 (s, 3H), 2.24 (s, 3H), 1.29 (s, 9H). ESI-MS: m/z = 392.1 $[M + H]^+$.

*4.1.55. N-(5-Bromo-6-((4-isopropoxyphenyl)amino)pyridin-2-yl)-pivalamide (**26c**).* General procedure G, yield: 71.3%. ESI-MS: m/z = 406 $[M + H]^+$.

*4.1.56. N-(6-((4-Methoxy-3-methylphenyl)amino)-5-phenylpyridin-2-yl)pivalamide (**26d**).* General procedure H, yield: 61.9%; ^{1}H NMR (400 MHz, $CDCl_3$) δ 7.83 (s, 1H), 7.58−7.50 (m, 3H), 7.50−7.42 (m, 3H), 7.30−7.24 (m, 1H), 7.13 (s, 1H), 6.86 (dd, J = 15.0, 8.3 Hz, 1H), 3.87 (s, 3H), 2.25 (s, 3H), 1.38 (s, 9H). ESI-MS: m/z = 390.0 $[M + H]^+$.

*4.1.57 N-(5-(4-Isopropoxyphenyl)-6-((4-methoxy-3-methylphenyl)amino)pyridin-2-yl)pivalamide (**26e**).* General procedure H, yield: 73.4%. ESI-MS: m/z = 448.0 $[M + H]^+$.

*4.1.58. N-(5-(4-Methoxy-3-methylphenyl)-6-((4-methoxy-3-methylphenyl)amino)pyridin-2-yl)pivalamide (**26f**).* General procedure H, yield: 69.9%; ^{1}H NMR (400 MHz, DMSO-d_6) δ 9.02 (s, 1H), 7.54 (dd, J = 8.8, 2.8 Hz, 1H), 7.31 (d, J = 2.7 Hz, 1H), 7.25 (dd, J = 8.4, 2.3 Hz, 1H), 7.23−7.17 (m, 2H), 7.06 (d, J = 8.4 Hz, 1H), 6.81 (d, J = 8.8 Hz, 1H), 6.62−6.50 (m, 1H), 2.22 (s, 3H), 2.13 (s, 3H), 1.28 (s, 9H). ESI-MS: m/z = 434.2 $[M + H]^+$.

*4.1.59. N-(6-((4-Methoxy-3-methylphenyl)amino)-5-(4-(trifluoromethyl)phenyl)pyridin-2-yl)pivalamide (**26g**).* General procedure H, yield: 81.5%; ^{1}H NMR (400 MHz, $CDCl_3$) δ 7.81 (s, 1H), 7.76 (d, J = 8.0 Hz, 2H), 7.61 (d, J = 8.0 Hz, 2H), 7.49 (d, J = 8.0 Hz, 1H), 7.23 (s, 1H), 7.11 (s, 1H), 6.82 (d, J = 8.7 Hz, 1H), 6.25 (s, 1H), 3.86 (s, 3H), 2.24 (s, 3H), 1.37 (s, 9H). ESI-MS: m/z = 458.0 $[M + H]^+$.

*4.1.60. N-(5-(4-Methoxy-3-methylphenyl)-6-(phenylamino)-pyridin-2-yl)pivalamide (**26h**).* General procedure H, yield: 84.9%. ESI-MS: m/z = 390.2 $[M + H]^+$.

*4.1.61. N-(6-((4-Isopropoxyphenyl)amino)-5-(4-methoxy-3-methylphenyl)pyridin-2-yl)pivalamide (**26i**).* General procedure H, yield: 18.1%. ESI-MS: m/z = 448.2 $[M + H]^+$.

*4.1.62. N^2-(4-Methoxy-3-methylphenyl)-3-phenylpyridine-2,6-diamine (**6g**).* General procedure I, yield: 72.3%; Melting point: 132−134 °C; retention time: 9.167 min; purity: 99.64%; ^{1}H NMR (400 MHz, $CDCl_3$) δ 7.49 (q, J = 5.9, 5.0 Hz, 4H), 7.40 (dt, J = 12.7, 5.2 Hz, 2H), 7.27 (d, J = 7.9 Hz, 1H), 7.18 (d, J = 2.8 Hz, 1H), 6.80 (d, J = 8.7 Hz, 1H), 6.37 (s, 1H), 6.06 (d, J = 7.9 Hz, 1H), 4.37 (s, 2H), 3.85 (s, 3H), 2.25 (s, 3H). ^{13}C NMR (100 MHz, $CDCl_3$) δ 156.7, 153.2, 152.0, 139.9, 138.6, 133.7, 129.3 × 4, 127.1, 126.8, 123.2, 118.6, 113.0, 110.5, 98.1, 55.8, 16.3. ESI-MS: m/z = 306.1 $[M + H]^+$. HRMS: calculated (M + H): 306.1606; found: 306.1610.

*4.1.63. 3-(4-Isopropoxyphenyl)-N^2-(4-methoxy-3-methylphenyl)-pyridine-2,6-diamine (**6h**).* General procedure I, yield: 91.1%; melting point: 95−96 °C; retention time: 11.393 min; purity: 98.81%; ^{1}H NMR (400 MHz, $CDCl_3$) δ 7.41 (dd, J = 8.7, 2.8 Hz, 1H), 7.38−7.32 (m, 2H), 7.23 (d, J = 7.9 Hz, 1H), 7.17 (d, J = 2.7 Hz, 1H), 7.00 (d, J = 8.6 Hz, 2H), 6.79 (d, J = 8.7 Hz, 1H), 6.35 (s, 1H), 6.04 (d, J = 7.8 Hz, 1H), 4.63 (hept, J = 6.1 Hz, 1H), 4.40 (s, 2H), 3.84 (s, 3H), 2.24 (s, 3H), 1.43 (d, J = 6.0 Hz, 6H). ^{13}C NMR (100 MHz, $CDCl_3$) δ 157.1, 156.3, 153.2, 152.1, 139.9, 133.7, 130.5 × 2, 130.3, 126.8, 123.1, 118.4, 116.4 × 2, 112.9, 110.5, 97.9, 70.0, 55.8, 29.7, 22.1 × 2. ESI-MS: m/z = 364.1 $[M + H]^+$. HRMS: calculated (M + H): 364.2025; found: 364.2030.

*4.1.64. N^2,3-Bis(4-methoxy-3-methylphenyl)pyridine-2,6-diamine (**6i**).* General procedure I, yield: 69.5%; melting point: 140−143 °C; retention time: 11.311 min; purity: 93.44%; ^{1}H NMR (400

https://doi.org/10.1021/acs.jmedchem.1c00586
J. Med. Chem. 2021, 64, 8621−8643

MHz, $CDCl_3$) δ 7.41 (dd, J = 8.7, 2.8 Hz, 1H), 7.29−7.24 (m, 1H), 7.25−7.21 (m, 2H), 7.20−7.17 (m, 1H), 6.94 (d, J = 8.2 Hz, 1H), 6.80 (d, J = 8.7 Hz, 1H), 6.39 (s, 1H), 6.04 (d, J = 7.9 Hz, 1H), 3.89 (d, J = 31.4 Hz, 6H), 2.28 (d, J = 27.7 Hz, 6H). ^{13}C NMR (100 MHz, $CDCl_3$) δ 157.0, 156.3, 153.1, 152.2, 139.9, 133.8, 131.7, 130.2, 127.7, 127.5, 126.8, 123.2, 118.5, 113.0, 110.5 × 2, 97.9, 55.8, 55.4, 16.3 × 2. ESI-MS: m/z = 350.1 $[M + H]^+$. HRMS: calculated (M + H): 350.1869; found: 350.1879.

*4.1.65. N^2-(4-Methoxy-3-methylphenyl)-3-(4-(trifluoromethyl)-phenyl)pyridine-2,6-diamine (**6j**).* General procedure I, yield: 75.2%; melting point: 131−132 °C; retention time: 11.041 min; purity: 100.00%; ^{1}H NMR (400 MHz, $CDCl_3$) δ 7.73 (d, J = 8.0 Hz, 2H), 7.60 (d, J = 8.0 Hz, 2H), 7.36 (dd, J = 8.7, 2.7 Hz, 1H), 7.26 (d, J = 8.0 Hz, 1H), 7.15 (d, J = 2.7 Hz, 1H), 6.80 (d, J = 8.7 Hz, 1H), 6.25 (s, 1H), 6.08 (d, J = 8.0 Hz, 1H), 4.44 (s, 2H), 3.85 (s, 3H), 2.24 (s, 3H). ^{13}C NMR (100 MHz, $CDCl_3$) δ 157.2, 153.5, 151.9, 142.5, 140.2, 133.2, 129.5 × 2, 126.9, 126.1 × 2, 123.6, 118.9, 111.3, 110.4, 98.4, 55.7, 16.2. ESI-MS: m/z = 374.1 $[M + H]^+$. HRMS: calculated (M + H): 374.1480; found: 374.1496.

*4.1.66. 3-(4-Methoxy-3-methylphenyl)-N^2-phenylpyridine-2,6-diamine (**6k**).* General procedure I, yield: 93.2%; melting point: 151−153 °C; retention time: 10.604 min; purity: 98.49%; ^{1}H NMR (400 MHz, $CDCl_3$) δ 7.56 (d, J = 7.9 Hz, 2H), 7.31 (d, J = 7.6 Hz, 2H), 7.28−7.24 (m, 2H), 7.04−6.90 (m, 2H), 6.58 (s, 1H), 6.10 (d, J = 7.9 Hz, 1H), 4.40 (s, 2H), 3.93 (s, 3H), 2.32 (s, 3H). ^{13}C NMR (100 MHz, $CDCl_3$) δ 157.1, 156.2, 151.5, 141.1, 140.0, 131.7, 129.9, 128.7 × 2, 127.7, 127.6, 121.3, 119.0 × 2, 113.6, 110.5, 98.6, 55.4, 16.3. ESI-MS: m/z = 306.1 $[M + H]^+$. HRMS: calculated (M + H): 306.1606; found: 306.1614.

*4.1.67. N^2-(4-Isopropoxyphenyl)-3-(4-methoxy-3-methylphenyl)-pyridine-2,6-diamine (**6l**).* General procedure I, yield: 67.6%; melting point: 130−133 °C; retention time: 12.060 min, purity: 95.63%; ^{1}H NMR (400 MHz, $CDCl_3$) δ 7.49−7.37 (m, 2H), 7.29−7.17 (m, 3H), 6.94 (d, J = 8.2 Hz, 1H), 6.93−6.81 (m, 2H), 6.43 (s, 1H), 6.05 (d, J = 7.9 Hz, 1H), 4.50 (hept, J = 6.1 Hz, 1H), 4.36 (s, 1H), 3.92 (s, 3H), 2.31 (s, 3H), 1.36 (d, J = 6.1 Hz, 6H). ^{13}C NMR (100 MHz, $CDCl_3$) δ 157.1, 156.3, 152.9, 152.0, 139.9, 134.4, 131.7, 130.1, 127.7, 127.5, 121.2 × 2, 116.6 × 2, 113.1, 110.5, 97.9, 70.6, 55.4, 29.7, 22.2 × 2. ESI-MS: m/z = 364.1 $[M + H]^+$. HRMS: calculated (M + H): 364.2025; found: 364.2032.

*4.1.68. N-Allyl-5,6-bis(4-methoxy-3-methylphenyl)pyridin-2-amine (**27**).* To a solution of compound **4** (12 mmol) and potassium *tert*-butoxide (17.8 mmol) in 40 mL of anhydrous THF was added allyl bromide (14 mmol) under a N_2 atmosphere. The mixture was stirred at room temperature for 12 h. After completion of the reaction, the mixture was concentrated under vacuum. To the residue was added 300 mL of water and extracted with ethyl acetate. The combined organic layers were washed with brine, dried over Na_2SO_4, and then concentrated under vacuum. The residue was purified by silica gel chromatography using ethyl acetate in petroleum ether (1:30−1:20) to afford the compound, yield: 40.0%; ^{1}H NMR (400 MHz, DMSO-d_6) δ 7.35 (d, J = 8.4 Hz, 1H), 7.21 (dd, J = 2.2, 0.9 Hz, 1H), 7.01 (dd, J = 8.5, 2.2 Hz, 1H), 6.93 (s, 1H), 6.85−6.77 (m, 2H), 6.74 (d, J = 8.5 Hz, 1H), 6.70 (t, J = 5.8 Hz, 1H), 6.49 (d, J = 8.4 Hz, 1H), 5.98 (ddt, J = 17.3, 10.4, 5.3 Hz, 1H), 5.26 (dq, J = 17.2, 1.8 Hz, 1H), 5.11 (dq, J = 10.3, 1.6 Hz, 1H), 3.97 (tt, J = 5.7, 1.6 Hz, 2H), 3.76 (d, J = 2.3 Hz, 6H), 2.08 (d, J = 7.2 Hz, 6H). ESI-MS: m/z = 375.0 $[M + H]^+$.

*4.1.69. 3-((5,6-Bis(4-methoxy-3-methylphenyl)pyridin-2-yl)-amino)propan-1-ol (**7a**) and 1-((5,6-bis(4-methoxy-3-methylphenyl)pyridin-2-yl)amino)propan-2-ol (**7b**).* To a solution of compound **23** (0.53 mmol) in 5 mL of anhydrous THF was added BH_3·THF (5.34 mmol). The mixture was stirred at room temperature for 1 h; then, 30% H_2O_2 (0.8 mmol) and 9 mL of 3 N NaOH were added and stirred overnight. After completion of the reaction, the mixture was poured into 100 mL of water and extracted with ethyl acetate. The combined organic layers were washed with brine, dried over Na_2SO_4, and then concentrated under vacuum. The residue was purified by silica gel chromatography using ethyl acetate in petroleum ether (1:8−1:2) to afford compounds **7a** and **7b**.

For compound **7a**, yield: 59.8%; retention time: 9.977 min; purity: 99.28%; ^{1}H NMR (400 MHz, $CDCl_3$) δ 7.46 (d, J = 8.4 Hz, 1H), 7.19 (d, J = 7.2 Hz, 2H), 7.02−6.96 (m, 1H), 6.89 (dd, J = 8.4, 2.3 Hz, 1H), 6.71 (dd, J = 8.8, 2.3 Hz, 2H), 6.42 (d, J = 8.4 Hz, 1H), 4.71 (s, 1H), 3.83 (d, J = 7.3 Hz, 6H), 3.66 (dt, J = 11.1, 6.2 Hz, 4H), 3.31 (s, 1H), 2.17 (d, J = 18.3 Hz, 6H), 1.83−1.75 (m, 2H). ^{13}C NMR (100 MHz, $CDCl_3$) δ 157.5, 157.3, 156.3, 154.3, 140.5, 132.7, 132.4, 132.1, 131.7, 128.4, 128.0, 126.2, 125.7, 124.8, 109.7, 109.2, 106.0, 58.7, 55.3 × 2, 38.0, 16.2 × 2, 14.2. ESI-MS: m/z = 393.1 $[M + H]^+$. HRMS: calculated (M + H): 393.2178; found: 393.2185.

For compound **7b**, yield: 36.5%; retention time: 9.920 min; purity: 100.00%; ^{1}H NMR (400 MHz, $CDCl_3$) δ 7.47 (d, J = 8.4 Hz, 1H), 7.17 (dd, J = 8.8, 1.6 Hz, 2H), 6.98 (dd, J = 2.3, 0.9 Hz, 1H), 6.88 (dd, J = 8.4, 2.3 Hz, 1H), 6.72 (d, J = 4.0 Hz, 1H), 6.70 (d, J = 3.6 Hz, 1H), 6.47 (d, J = 8.4 Hz, 1H), 5.04 (d, J = 6.0 Hz, 1H), 4.05 (pd, J = 6.4, 2.4 Hz, 1H), 3.83 (d, J = 6.3 Hz, 6H), 3.55 (ddd, J = 14.2, 5.6, 2.4 Hz, 1H), 3.36 (ddd, J = 14.0, 6.9, 5.0 Hz, 1H), 2.17 (d, J = 17.9 Hz, 6H), 1.25 (d, J = 6.3 Hz, 3H). ^{13}C NMR (100 MHz, $CDCl_3$) δ 157.3, 156.3, 154.1, 140.7, 132.6, 132.2, 132.1, 131.7, 128.4, 128.0, 126.2, 125.7, 125.3, 109.7, 109.3, 106.3, 68.3, 55.3 × 2, 50.7, 20.9, 16.2 × 2. ESI-MS: m/z = 393.1 $[M + H]^+$.

*4.1.70. N-(5,6-Bis(4-methoxy-3-methylphenyl)pyridin-2-yl)-3-chloropropanamide (**28**).* To a solution of compound **4** (1.49 mmol) and TEA (4.5 mmol) in 15 mL of DCM was added 3-chloropropionyl (3 mmol) dropwise at 0 °C. The mixture was moved to room temperature and reacted for 5 h. After completion of this reaction, the mixture was poured into 100 mL of water and extracted with ethyl acetate. The combined organic layers were washed with brine, dried over Na_2SO_4, and then concentrated under vacuum. The residue was purified by silica gel chromatography using ethyl acetate in petroleum ether (1:10−1:4) to afford the compound, yield: 67.7%; ^{1}H NMR (400 MHz, $CDCl_3$) δ 8.49 (s, 1H), 8.29 (d, J = 8.4 Hz, 1H), 7.78 (d, J = 8.4 Hz, 1H), 7.29 (dd, J = 2.4, 1.0 Hz, 1H), 7.08 (dd, J = 8.5, 2.3 Hz, 1H), 7.04 (dd, J = 2.3, 1.0 Hz, 1H), 6.95 (dd, J = 8.4, 2.3 Hz, 1H), 6.75 (d, J = 8.4 Hz, 1H), 6.70 (d, J = 8.5 Hz, 1H), 6.52 (dd, J = 16.9, 1.2 Hz, 1H), 6.31 (dd, J = 16.9, 10.2 Hz, 1H), 5.85 (dd, J = 10.2, 1.2 Hz, 1H), 3.85 (d, J = 7.1 Hz, 6H), 2.21 (d, J = 3.1 Hz, 6H). ESI-MS: m/z = 425.0 $[M + H]^+$.

*4.1.71. N-(5,6-Bis(4-methoxy-3-methylphenyl)pyridin-2-yl)-3-(4-hydroxypiperidin-1-yl)propenamide (**7c**).* General procedure J, yield: 87.1%; melting point: 62−64 °C; retention time: 10.123 min; purity: 99.65%; ^{1}H NMR (400 MHz, $CDCl_3$) δ 11.42 (s, 1H), 8.11 (d, J = 8.3 Hz, 1H), 7.67 (d, J = 8.3 Hz, 1H), 7.40 (dd, J = 2.3, 1.0 Hz, 1H), 7.10 (dd, J = 8.5, 2.3 Hz, 1H), 7.05 (dd, J = 2.3, 1.0 Hz, 1H), 6.96 (dd, J = 8.4, 2.3 Hz, 1H), 6.75 (d, J = 8.3 Hz, 1H), 6.64 (d, J = 8.5 Hz, 1H), 3.91−3.86 (m, 1H), 3.84 (d, J = 13.2 Hz, 6H), 2.95 (dt, J = 10.9, 4.5 Hz, 2H), 2.81 (t, J = 6.0 Hz, 2H), 2.60 (t, J = 6.0 Hz, 2H), 2.43 (s, 2H), 2.20 (d, J = 8.7 Hz, 6H), 2.09 (p, J = 3.7 Hz, 2H), 1.84 (dtd, J = 12.5, 8.7, 3.6 Hz, 2H), 1.73 (s, 1H). ^{13}C NMR (100 MHz, $CDCl_3$) δ 171.0, 157.5, 156.8, 154.4, 150.1, 140.9, 132.3, 132.2, 131.9, 131.6, 131.2, 128.8, 128.0, 126.5, 125.7, 111.6, 109.8, 108.9, 67.3, 55.3 × 2, 53.3, 50.0 × 2, 34.3 × 2, 33.4, 16.2 × 2. ESI-MS: m/z = 490.0 $[M + H]^+$.

*4.1.72. N-(5,6-Bis(4-methoxy-3-methylphenyl)pyridin-2-yl)-3-morpholinopropanamide (**7d**).* General procedure J, yield: 89.6%; melting point: 78−80 °C; retention time: 11.182 min; purity: 99.74%; ^{1} H NMR (400 MHz, $CDCl_3$) δ 11.09 (s, 1H), 8.12 (d, J = 8.4 Hz, 1H), 7.68 (d, J = 8.4 Hz, 1H), 7.41−7.35 (m, 1H), 7.13 (dd, J = 8.5, 2.3 Hz, 1H), 7.08−7.01 (m, 1H), 6.97 (dd, J = 8.4, 2.3 Hz, 1H), 6.76 (d, J = 8.4 Hz, 1H), 6.67 (d, J = 8.5 Hz, 1H), 3.92 (t, J = 4.6 Hz, 4H), 3.85 (d, J = 8.4 Hz, 6H), 2.82 (t, J = 6.0 Hz, 2H), 2.68 (t, J = 4.4 Hz, 4H), 2.61 (t, J = 6.0 Hz, 2H), 2.21 (d, J = 10.3 Hz, 6H). ^{13}C NMR (100 MHz, $CDCl_3$) δ 171.0, 157.5, 156.8, 154.4, 150.1, 140.9, 132.3, 132.2, 131.9, 131.6, 131.2, 128.8, 128.0, 126.5, 125.7, 111.6, 109.8, 108.9, 67.3, 55.3 × 2, 53.3, 50.0 × 2, 34.3 × 2, 33.4, 16.2 × 2. ESI-MS: m/z = 476.0 $[M + H]^+$. HRMS: calculated (M + H): 476.2549; found: 476.2553.

*4.1.73. N-(5,6-Bis(4-methoxy-3-methylphenyl)pyridin-2-yl)-3-(1H-1,2,4-triazol-1-yl)propenamide (**7e**).* General procedure J, yield: 70.3%; retention time: 15.827 min; purity: 100.00%; ^{1}H

https://doi.org/10.1021/acs.jmedchem.1c00586
J. Med. Chem. 2021, 64, 8621−8643

NMR (400 MHz, $CDCl_3$) δ 8.98 (s, 1H), 8.14 (s, 1H), 8.06 (d, J = 8.4 Hz, 1H), 7.90 (s, 1H), 7.69 (d, J = 8.4 Hz, 1H), 7.19 (d, J = 2.2 Hz, 1H), 7.03−6.95 (m, 2H), 6.89 (dd, J = 8.4, 2.3 Hz, 1H), 6.70 (d, J = 8.4 Hz, 1H), 6.60 (d, J = 8.5 Hz, 1H), 4.48 (t, J = 6.2 Hz, 2H), 3.79 (d, J = 12.5 Hz, 6H), 2.73 (t, J = 6.2 Hz, 2H), 2.13 (d, J = 22.9 Hz, 6H). ^{13}C NMR (100 MHz, $CDCl_3$) δ 168.1, 157.7, 157.0, 154.8, 152.1, 149.1, 143.9, 141.3, 132.2, 132.0, 131.6, 131.4, 131.3, 128.6, 128.0, 126.6, 126.2, 112.0, 109.7, 109.2, 55.3 × 2, 44.8, 29.7, 16.2 × 2. ESI-MS: m/z = 458 $[M + H]^+$. HRMS: calculated (M +H): 458.2192; found: 458.2200.

*4.1.74. 5,6-Bis(4-methoxy-3-methylphenyl)-N-(3-morpholinopropyl)pyridin-2-amine (**7f**).* To a mixture of $LiAlH_4$ (0.63 mmol) in 5 mL anhydrous THF was added compound **7d** (0.11 mmol) at 0 °C under a N_2 atmosphere. Then, the mixture was moved to room temperature and stirred for 10 h. The reaction was quenched by adding 24 μL of H_2O, 24 μL of 15% NaOH, and 72 μL of H_2O in sequence. Then, the mixture was filtered and the filtrate was concentrated under vacuum. The residue was purified through chromatography to afford the compound, yield: 63.2%; retention time: 7.380 min; purity: 98.60%; ^{1}H NMR (400 MHz, $CDCl_3$) δ 7.50 (d, J = 8.4 Hz, 1H), 7.34−7.28 (m, 1H), 7.11 (dd, J = 8.4, 2.3 Hz, 1H), 7.00 (dd, J = 2.2, 0.9 Hz, 1H), 6.90 (dd, J = 8.4, 2.3 Hz, 1H), 6.69 (dd, J = 18.6, 8.4 Hz, 2H), 6.44 (d, J = 8.4 Hz, 1H), 3.84 (d, J = 6.4 Hz, 6H), 3.79 (t, J = 4.7 Hz, 4H), 3.46 (t, J = 6.6 Hz, 2H), 2.60−2.50 (m, 6H), 2.20 (d, J = 5.0 Hz, 6H), 1.90 (p, J = 6.8 Hz, 2H). ^{13}C NMR (100 MHz, $CDCl_3$) δ 157.3, 156.3, 154.5, 140.6, 132.9, 132.6, 132.1, 131.7, 128.6, 128.0, 126.2, 125.7, 124.8, 109.7, 109.1, 104.2, 67.0 × 2, 56.9, 55.3 × 2, 53.8 × 2, 41.1, 26.2, 16.2 × 2. ESI-MS: m/z = 462.2 $[M + H]^+$. HRMS: calculated (M + H): 462.2757; found: 462.2765.

*4.1.75. N-(2-Fluoro-5-nitrophenyl)benzamide (**31a**).* General procedure K, yield: 56.8%; ^{1}H NMR (400 MHz, DMSO-d_6) δ 10.49 (s, 1H), 8.67 (dd, J = 6.5, 2.9 Hz, 1H), 8.17 (ddd, J = 9.0, 4.0, 3.0 Hz, 1H), 8.03−7.95 (m, 2H), 7.65 (td, J = 5.2, 2.2 Hz, 1H), 7.63−7.51 (m, 3H). ESI-MS: m/z = 260.8 $[M + H]^+$.

*4.1.76. N-(2-Fluoro-5-nitrophenyl)-4-methoxy-3-methylbenzamide (**31b**).* General procedure K, yield: 63.8%; ^{1}H NMR (400 MHz, $CDCl_3$) δ 9.46 (dd, J = 6.8, 2.7 Hz, 1H), 8.08 (s, 1H), 7.99 (ddd, J = 7.5, 4.0, 3.1 Hz, 1H), 7.76 (dd, J = 8.5, 2.2 Hz, 1H), 7.69 (s, 1H), 7.27 (t, J = 9.5 Hz, 1H), 6.91 (d, J = 8.5 Hz, 1H), 3.91 (s, 3H), 2.28 (s, 3H). ESI-MS: m/z = 305.0 $[M + H]^+$.

*4.1.77. N-(2-(4-Hydroxypiperidin-1-yl)-5-nitrophenyl)-4-methoxy-3-methylbenzamide (**8a**).* General procedure L, yield: 94.2%; melting point: 188−190 °C; ^{1}H NMR (400 MHz, DMSO-d_6) δ 9.45 (s, 1H), 8.72 (d, J = 2.1 Hz, 1H), 7.99 (dd, J = 8.7, 1.9 Hz, 1H), 7.86 (d, J = 8.0 Hz, 1H), 7.79 (s, 1H), 7.30 (d, J = 8.9 Hz, 1H), 7.10 (d, J = 8.5 Hz, 1H), 4.57 (s, 1H), 3.88 (s, 3H), 3.77−3.57 (m, 1H), 3.22 (d, J = 11.6 Hz, 2H), 2.84 (t, J = 9.8 Hz, 2H), 2.22 (s, 3H), 1.87 (d, J = 9.5 Hz, 2H), 1.72−1.48 (m, 2H). ^{13}C NMR (100 MHz, DMSO-d_6) δ 164.9, 160.9, 151.6, 142.1, 131.8, 130.2, 127.3, 126.3, 125.9, 121.0, 120.3, 118.9, 110.6, 65.8, 56.1, 48.9 × 2, 34.9 × 2, 16.6. ESI-MS: m/z = 386.0 $[M + H]^+$. HRMS: calculated (M + H): 386.1716; found: 386.1719.

*4.1.78. 4-Methoxy-3-methyl-N-(2-(4-methylpiperazin-1-yl)-5-nitrophenyl)benzamide (**8b**).* General procedure L, yield: 56.8%; melting point: 187−189 °C; ^{1}H NMR (400 MHz, $CDCl_3$) δ 9.40 (d, J = 2.6 Hz, 1H), 9.07 (s, 1H), 7.96 (dd, J = 8.7, 2.7 Hz, 1H), 7.79 (dd, J = 8.5, 2.2 Hz, 1H), 7.74 (s, 1H), 7.28 (d, J = 1.8 Hz, 1H), 6.95 (d, J = 8.5 Hz, 1H), 3.94 (s, 3H), 3.05 (t, J = 4.7 Hz, 4H), 2.96−2.53 (m, 4H), 2.44 (s, 3H), 2.32 (s, 3H). ^{13}C NMR (100 MHz, $CDCl_3$) δ 164.6, 161.1, 146.9, 144.9, 134.0, 129.4, 127.3, 126.5, 125.8, 120.3, 118.9, 114.8, 109.8, 55.7 × 2, 55.6, 51.6 × 2, 46.1, 16.4. ESI-MS: m/z = 385.0 $[M + H]^+$. HRMS: calculated (M + H): 385.1876; found: 385.1883.

*4.1.79. 4-Methoxy-3-methyl-N-(2-morpholino-5-nitrophenyl)-benzamide (**8c**).* General procedure L, yield: 70.8%; melting point: 210−213 °C; ^{1}H NMR (400 MHz, $CDCl_3$) δ 9.37 (d, J = 2.6 Hz, 1H), 9.05 (s, 1H), 7.95 (dd, J = 8.7, 2.6 Hz, 1H), 7.75 (dd, J = 8.5, 2.1 Hz, 1H), 7.70 (s, 1H), 7.25 (d, J = 8.8 Hz, 1H), 6.92 (t, J = 7.3 Hz, 1H), 3.97−3.93 (m, 4H), 3.92 (s, 3H), 3.06−2.95 (m, 4H), 2.30 (s, 3H). ^{13}C NMR (100 MHz, $CDCl_3$) δ 164.6, 161.2, 146.6, 145.0, 134.0, 129.4, 127.4, 126.3, 125.7, 120.3, 119.0, 115.0, 109.8, 67.4 × 2, 55.6, 52.0 × 2, 16.5. ESI-MS: m/z = 372.0 $[M + H]^+$. HRMS: calculated (M + H): 372.1559; found: 372.1564.

*4.1.80. N-(2-(4-Hydroxypiperidin-1-yl)-5-nitrophenyl)benzamide (**8d**).* General procedure L, yield: 93.2%; melting point: 188−190 °C; ^{1}H NMR (400 MHz, DMSO-d_6) δ 9.68 (s, 1H), 8.68 (d, J = 2.7 Hz, 1H), 8.03 (dd, J = 9.1, 2.9 Hz, 2H), 7.99 (d, J = 1.5 Hz, 1H), 7.68−7.61 (m, 1H), 7.57 (dd, J = 11.4, 4.4 Hz, 2H), 7.30 (d, J = 9.0 Hz, 1H), 4.79 (d, J = 3.9 Hz, 1H), 3.67 (dt, J = 11.4, 3.7 Hz, 1H), 3.31−3.18 (m, 2H), 2.96−2.77 (m, 2H), 1.93−1.78 (m, 2H), 1.65−1.49 (m, 2H). ^{13}C NMR (100 MHz, DMSO-d_6) δ 165.4, 152.1, 141.8, 134.4, 132.6, 131.2, 129.2 × 2, 127.8 × 2, 121.5, 120.2, 119.8, 65.8, 48.8 × 2, 34.8 × 2. ESI-MS: m/z = 342.0 $[M + H]^+$. HRMS: calculated (M + H): 342.1454; found: 342.1460.

*4.1.81. N-(2-(4-Methylpiperazin-1-yl)-5-nitrophenyl)benzamide (**8e**).* General procedure L, yield: 73.6%; melting point: 166−169 °C; ^{1}H NMR (400 MHz, $CDCl_3$) δ 9.40 (d, J = 2.6 Hz, 1H), 9.12 (s, 1H), 7.97 (dd, J = 8.8, 2.7 Hz, 1H), 7.95−7.88 (m, 2H), 7.63−7.58 (m, 1H), 7.55 (t, J = 7.3 Hz, 2H), 7.30−7.26 (m, 1H), 3.03 (t, J = 4.7 Hz, 4H), 2.65 (m, 4H), 2.40 (s, 3H). ^{13}C NMR (100 MHz, $CDCl_3$) δ 165.0, 147.3, 145.0, 134.3, 133.8, 132.5, 129.2 × 2, 127.1 × 2, 120.5, 119.5, 115.1, 55.8 × 2, 51.9 × 2, 46.2. ESI-MS: m/z = 341.0 $[M + H]^+$. HRMS: calculated (M + H): 341.1614; found: 341.1622.

*4.1.82. N-(2-Morpholino-5-nitrophenyl)benzamide (**8f**).* General procedure L, yield: 37.3%; melting point: 218−220 °C; ^{1}H NMR (400 MHz, DMSO-d_6) δ 9.81 (s, 1H), 8.71 (d, J = 2.7 Hz, 1H), 8.06 (dt, J = 8.2, 4.1 Hz, 1H), 8.01−7.97 (m, 2H), 7.64 (dd, J = 8.4, 6.1 Hz, 1H), 7.57 (dd, J = 15.2, 8.2 Hz, 2H), 7.35 (d, J = 9.0 Hz, 1H), 3.84−3.72 (m, 4H), 3.13−3.01 (m, 4H). ^{13}C NMR (100 MHz, DMSO-d_6) δ 165.0, 150.8, 141.9, 133.8, 132.1, 131.1, 128.8 × 2, 127.4 × 2, 121.1, 120.0, 119.5, 66.1 × 2, 50.6 × 2. ESI-MS: m/z = 328.0 $[M + H]^+$.

*4.1.83. N-(5-Amino-2-(4-hydroxypiperidin-1-yl)phenyl)-4-methoxy-3-methylbenzamide (**8g**).* General procedure M, yield: 43.6%; melting point: 181−183 °C; ^{1}H NMR (400 MHz, DMSO-d_6) δ 9.60 (s, 1H), 7.72 (dd, J = 8.5, 2.0 Hz, 1H), 7.68 (d, J = 8.0 Hz, 1H), 7.66 (d, J = 2.5 Hz, 1H), 7.11 (d, J = 8.6 Hz, 1H), 6.96 (d, J = 8.4 Hz, 1H), 6.26 (dd, J = 8.4, 2.5 Hz, 1H), 5.00 (s, 2H), 4.75 (d, J = 3.9 Hz, 1H), 3.87 (s, 3H), 3.61 (dt, J = 26.9, 13.4 Hz, 1H), 2.82 (d, J = 11.8 Hz, 2H), 2.63 (t, J = 9.7 Hz, 2H), 2.23 (s, 3H), 1.87 (d, J = 9.9 Hz, 2H), 1.57 (td, J = 12.5, 3.4 Hz, 2H). ^{13}C NMR (100 MHz, DMSO-d_6) δ 163.6, 160.6, 146.5, 134.4, 131.9, 129.6, 127.1, 126.5, 126.5, 121.8, 110.7, 109.1, 104.9, 66.2, 56.1 × 2, 51.4, 36.2, 16.7 × 2. ESI-MS: m/z = 356.0 $[M + H]^+$. HRMS: calculated (M + H): 356.1974; found: 356.1986.

*4.1.84. N-(5-Amino-2-(4-methylpiperazin-1-yl)phenyl)-4-methoxy-3-methylbenzamide (**8h**).* General procedure M, yield: 44.8%; ^{1}H NMR (400 MHz, $CDCl_3$) δ 9.66 (s, 1H), 8.01 (d, J = 2.6 Hz, 1H), 7.78 (dt, J = 10.6, 5.3 Hz, 1H), 7.73 (d, J = 1.8 Hz, 1H), 7.03 (d, J = 8.4 Hz, 1H), 6.92 (d, J = 8.5 Hz, 1H), 6.38 (dd, J = 8.4, 2.7 Hz, 1H), 3.90 (s, 3H), 3.10−2.87 (m, 4H), 2.86−2.40 (m, 4H), 2.38 (s, 3H), 2.30 (s, 3H). ^{13}C NMR (100 MHz, $CDCl_3$) δ 164.5, 160.6, 144.6, 135.0, 132.4, 129.4, 127.0, 126.9, 126.5, 121.9, 109.6, 109.5, 105.7, 56.5 × 2, 55.5, 52.7 × 2, 46.3, 16.4. ESI-MS: m/z = 355.1 $[M + H]^+$. HRMS: calculated (M + H): 355.2134; found: 355.2136.

*4.1.85. N-(5-Amino-2-morpholinophenyl)-4-methoxy-3-methylbenzamide (**8i**).* General procedure M, yield: 73.9%; ^{1}H NMR (400 MHz, $CDCl_3$) δ 9.66 (s, 1H), 8.06 (d, J = 2.6 Hz, 1H), 7.80 (dt, J = 7.2, 3.6 Hz, 1H), 7.75 (d, J = 8.8 Hz, 1H), 7.07 (d, J = 8.4 Hz, 1H), 6.96 (d, J = 8.5 Hz, 1H), 6.44 (dd, J = 8.4, 2.6 Hz, 1H), 3.94 (s, 3H), 3.90 (t, J = 13.0 Hz, 4H), 2.99−2.84 (m, 4H), 2.34 (s, 3H). ^{13}C NMR (100 MHz, $CDCl_3$) δ 164.6, 160.7, 144.9, 135.1, 132.3, 129.5, 127.2, 127.0, 126.3, 122.0, 109.7, 109.7, 105.9, 68.2 × 2, 55.6, 53.3 × 2, 16.6. ESI-MS: m/z = 342.1 $[M + H]^+$.

4.2. Cell Culture and Plasmids. The NCI-H1299, H460, KHOS, A2780, and 293T cell lines were purchased from the Cell Bank of Type Culture Collection of the Chinese Academy of Sciences (Shanghai, China). All cells were cultured in Dulbecco's modified

https://doi.org/10.1021/acs.jmedchem.1c00586
J. Med. Chem. 2021, 64, 8621−8643

Eagle's medium (DMEM) or RPMI-1640 medium supplemented with 10% fetal bovine serum (FBS; Gibco) in a humidified atmosphere of 5% CO_2 at 37°C. The full-length coding sequence for WSB1 and RhoGDI2 was amplified from the U2OS cDNA library and subsequently subcloned into the pCDH plasmid (Addgene).

4.3. Antiproliferation Assay. H460 or KHOS cells were seeded in 96-well plates at a density of 5000 cells per well. After 24 h, cells were incubated with a medium alone or a medium containing test compounds for 16 h or 48 h. Serial concentrations of both compounds were added into the wells. Cell viability was determined by the methyl thiazolyl tetrazolium (MTT) or CCK8 assay. Growth inhibition was calculated as % = $[1 - (A/B)] \times 100$, where A and B are the absorbance of treated and untreated cells, respectively.

4.4. Transwell Assay. Under a hypoxic or normoxic environment, the cell migration assay was performed in a 24-well transwell plate with 8 μm of polycarbonate sterile membrane (Corning Incorporated). Cells were plated in the upper chamber at 2×10^4 cells per insert in 200 μL of serum-free medium. Inserts were placed in wells containing 600 μL of medium supplemented with 10% FBS. After being cultured for 24 h, cells on the upper surface were detached with a cotton swab. Filters were fixed, and cells in the lower filter were stained with 0.1% crystal violet for 15 min and photographed, under a 100× microscope. Three different visual fields were chosen randomly to take the count of the number of cells. The migration rate was normalized to the control: migration rate = A/B (A = number of migration cells in the dosing group; B = number of migration cells in the control group)

4.5. Wound-Healing Assay. Cells (5×10^5 cell/well) were seeded in a 24-well plate until they attached and formed a monolayer on plates. A straight band of cells was scraped using a pipette tip. After being scraped, the cells were washed with phosphate-buffered saline (PBS) and were subsequently exposed to 1‰ DMSO or tested compounds. The migration of cells across this artificial wound was assessed at different time intervals by microscopic observation. The cell migration rate was calculated as $(C - D)/(A - B)$ (A = blank area of the control, 0 h; B = blank area of the control, 16, 24, or 48 h; C = blank area of the compound, 0 h; D = blank area of the compound, 16, 24, or 48 h).

4.6. Western Blotting. Cells were harvested and lysed in a 2× sodium dodecyl sulfate (SDS) gel loading buffer [24 mM Tris-HCl (pH 6.8), 0.02% mercaptoethanol, 4% SDS, 0.4% bromphenol blue, 20% glycerol]. Equal volumes of cell lysates were resolved on 8−12% SDS-polyacrylamide gel electrophoresis (PAGE) gels and transferred to poly(vinylidene difluoride) (PVDF) membranes (Pierce Chemical). The blots were incubated for 1 h in a TBS-T solution supplemented with 5% nonfat dry milk. Membranes were probed with the specific primary antibodies, followed by horseradish peroxidase-conjugated secondary antibodies. The bands were visualized by chemiluminescence (Perkinelmer). The primary antibody for β-actin was from Santa Cruz Biotechnology (Santa Cruz, CA), Myc-tag and Flag-tag were obtained from Cell Signaling Technology (Beverly, MA), and RhoGDI2 was from Spring Bioscience (Pleasanton, CA). Secondary antibodies were from Fude Biological Technology.

4.7. RT-PCR Analysis. Total RNA was extracted with the EasyPure RNA kit according to the manufacturer's protocol (Transgen Biotech), and cDNA was synthesized with TranScript One-Step gDNA Removal and cDNA Systhesis SuperMix (Transgen Biotech). The relative mRNA levels were evaluated by quantitative RT-PCR using Eppendorfep Gradient Mastercycler (Eppendorf, Hamburg, Germany) and Bio-Rad SYBR Green Master Mix. Primers used were as follows: GAPDH, forward primer: 5′-GTCATCCATGACAACTTTGG-3′ and reverse primer: 5′-GAGCTTGACAAAGTGGTCGT-3′; WSB1, forward primer: 5′-CGTACTATAGGTGAACTTTTAGCTCCT-3′ and reverse primer: 5′-CCAAAGGAAAACTGCTTTACTGG-3′; RhoGDI2, forward primer: 5′-CCCTGGTTTGTGAGAGTGC-3′ and reverse primer: 5′-GGCCTGACACAATATCCCTG-3′.

4.8. Immunoprecipitation. The transfected 293T cells were harvested and lysed by IP buffer (0.5% NP-40, 0.5% Triton X-100, 150 mM NaCl, 50 mM Tris-HCl, 2 mM ethylenediaminetetraacetic acid (EDTA), 2 mM ethylene glycol tetraacetic acid (EGTA), 25 mM NaF, 25 mM glycero-2-phosphate disodium salt, 0.1% Cocktail, pH = 7.5). After centrifuging with the speed of 12 000g for 30 min at 4 °C, the supernatant was obtained. The cell lysate (2−3 mg from harvested cells) was incubated with 20 μL of suspension of anti-FLAG beads for 6 h at 4 °C. After centrifugation at 500g for 2 min at 4 °C, the beads were washed five times with 500 μL of washing buffer (25 mM Tris, 150 mM NaCl, 0.2% Nonidet P-40, pH = 8.0), and proteins were dissociated from beads by 2.5× loading buffer.

4.9. F-Actin Staining Assay and Confocal Microscopy. H1299-WSB1 cells were planted into the 24-well plate containing cell slides and treated with compound **4** (20 μM) for 24 h. After that, cells were fixed with 4% paraformaldehyde for 15 min at 4°C and then permeabilized with 0.1% Triton X-100 in PBS for 10 min. The cells were then blocked with 1% bovine serum albumin (BSA) for 20 min and incubated with Texas Red-X phalloidin (Life Technologies) diluted according to the dilution ratio of 1:40 in PBS for 20 min. Cells were stained with 4′,6-diamidino-2-phenylindole (DAPI; 100 mg/mL) for 3 min. The slides were mounted with antifade reagent. The cells were observed and photographed under a confocal microscope (Leica-TCS SP8).

4.10. Animals. Sprague−Dawley (SD) rats (male, 8 weeks old, 250−300 g) were purchased from Zhejiang Laboratory Animal Center (Hangzhou, China). Balb/c mice (nu/nu, female, 3−4 weeks old, 20−25 g) were purchased from the National Rodent Laboratory Animal Resource (Shanghai, China). These animals were bred at the College of Pharmaceutical Sciences, Zhejiang University. The animals were maintained under a 12 h light−dark cycle with free access to water and food. All animal studies were performed in strict accordance with the institutional guidelines as defined by the Institutional Animal Care and Use Committee (IUCAC) and approved by the Animal Care and Use Committee, Zhejiang University Laboratory Animal Center (Hangzhou, China).

4.11. Pharmacokinetic Studies. SD rats were administered compound **4** 100 mg/kg p.o. or 160 mg/kg ip in the solvent (2% DMSO + 98% (0.5% methyl cellulosem (MC))). Three rats were dosed in each group. Venous blood (100 μL) samples were collected at 0.25, 0.5, 1, 2, 4, 6, 8, and 24 h. Plasma was separated from whole blood by centrifugation and stored at −20°C until analysis. Compound levels were determined by API4000+ LC/MS. The C_{max}, T_{max}, $t_{1/2}$, and AUC were evaluated using Analyst 1.5.1.

4.12. Measurement of *In Vivo* Activity. Balb/c (nu/nu) mice were maintained in a pathogen-free animal facility. Tumors were established via armpit injection of 4T1 cells (1×10^7 cells/animal) into the 3- to 4-week-old female Balb/c (nu/nu) mice. When tumors reached 100−200 mm^3, the mice were randomly divided into control and treatment groups to receive one of the following daily treatments for 28 days: vehicle (phosphate-buffered saline (PBS), po), **4** (100 mg/kg, po); Taxol (10 mg/kg, ip). Six mice were included in each group. Tumor volume (V) was calculated as $V = (\text{length} \times \text{width}^2)/2$. The relative tumor volume (RTV) was calculated as RTV = V_n/V_0 (V_n is tumor volume on days n; V_0 is tumor volume on the first day of treatment). After completion of the treatment, mice were sacrificed. The lung tissues were dissected, formalin-fixed, and paraffin-embedded. Then, they were cut into slices and stained with hematoxylin/eosin. The lung metastasis foci were observed and counted under a microscope.

4.13. Statistical Analysis. Statistical analysis was performed using GraphPad Prism 5 software (GraphPad software, Inc, La Jolla, CA). Unless otherwise stated, the values for all samples in the different experimental conditions were averaged, and the standard deviation of the mean was calculated. Statistical differences between two groups were assessed by Student's t-test. A P value of less than 0.05 was considered statistically significant.

■ ASSOCIATED CONTENT

Supporting Information

The Supporting Information is available free of charge at https://pubs.acs.org/doi/10.1021/acs.jmedchem.1c00586.

https://doi.org/10.1021/acs.jmedchem.1c00586
J. Med. Chem. 2021, 64, 8621−8643

Structures of representative compounds from an in-house structurally diverse library (Figure S1); relative mRNA levels of RhoGDI2 and WSB1 in H1299-WSB1 cells (Figure S2); purification of WSB1 protein using whole-cell lysate (Figure S3); representative figures of the wound-healing assay of compounds **1a** and **4** against KHOS cells (Table S1); representative figures of the wound-healing assay of compounds **1a** and **4** against H460 cells (Table S2); and NMR spectra and HPLC results for the target compounds (PDF)

Molecular formula strings (CSV)

AUTHOR INFORMATION

Corresponding Authors

Xiaowu Dong − *Hangzhou Institute of Innovative Medicine, Institute of Drug Discovery and Design, College of Pharmaceutical Sciences, Zhejiang University, Hangzhou 310058, P. R. China; Innovation Institute for Artificial Intelligence in Medicine of Zhejiang University, Hangzhou 310018, P. R. China; Cancer Center, Zhejiang University, Hangzhou 310058, P. R. China;* orcid.org/0000-0002-2178-4372; Email: dongxw@zju.edu.cn

Ji Cao − *Institute of Pharmacology & Toxicology, Zhejiang Province Key Laboratory of Anti-Cancer Drug Research, College of Pharmaceutical Sciences and Cancer Center, Zhejiang University, Hangzhou 310058, P. R. China; Innovation Institute for Artificial Intelligence in Medicine of Zhejiang University, Hangzhou 310018, P. R. China;* Email: caoji88@zju.edu.cn

Authors

Jinxin Che − *Hangzhou Institute of Innovative Medicine, Institute of Drug Discovery and Design, College of Pharmaceutical Sciences, Zhejiang University, Hangzhou 310058, P. R. China*

Zegao Jin − *Hangzhou Institute of Innovative Medicine, Institute of Drug Discovery and Design, College of Pharmaceutical Sciences, Zhejiang University, Hangzhou 310058, P. R. China*

Fangjie Yan − *Institute of Pharmacology & Toxicology, Zhejiang Province Key Laboratory of Anti-Cancer Drug Research, College of Pharmaceutical Sciences, Zhejiang University, Hangzhou 310058, P. R. China; Innovation Institute for Artificial Intelligence in Medicine of Zhejiang University, Hangzhou 310018, P. R. China*

Jieqiong You − *Institute of Pharmacology & Toxicology, Zhejiang Province Key Laboratory of Anti-Cancer Drug Research, College of Pharmaceutical Sciences, Zhejiang University, Hangzhou 310058, P. R. China*

Jiangfeng Xie − *Hangzhou Institute of Innovative Medicine, Institute of Drug Discovery and Design, College of Pharmaceutical Sciences, Zhejiang University, Hangzhou 310058, P. R. China*

Binhui Chen − *Hangzhou Institute of Innovative Medicine, Institute of Drug Discovery and Design, College of Pharmaceutical Sciences, Zhejiang University, Hangzhou 310058, P. R. China*

Gang Cheng − *College of Pharmaceutical Science, Zhejiang Chinese Medical University, Hangzhou 311402, P. R. China;* orcid.org/0000-0002-1760-9539

Hong Zhu − *Institute of Pharmacology & Toxicology, Zhejiang Province Key Laboratory of Anti-Cancer Drug Research, College of Pharmaceutical Sciences and Cancer Center, Zhejiang University, Hangzhou 310058, P. R. China*

Qiaojun He − *Hangzhou Institute of Innovative Medicine, Institute of Drug Discovery and Design, College of Pharmaceutical Sciences, Zhejiang University, Hangzhou 310058, P. R. China; Institute of Pharmacology & Toxicology, Zhejiang Province Key Laboratory of Anti-Cancer Drug Research, College of Pharmaceutical Sciences and Cancer Center, Zhejiang University, Hangzhou 310058, P. R. China; Innovation Institute for Artificial Intelligence in Medicine of Zhejiang University, Hangzhou 310018, P. R. China*

Yongzhou Hu − *Hangzhou Institute of Innovative Medicine, Institute of Drug Discovery and Design, College of Pharmaceutical Sciences, Zhejiang University, Hangzhou 310058, P. R. China;* orcid.org/0000-0001-7349-4062

Bo Yang − *Institute of Pharmacology & Toxicology, Zhejiang Province Key Laboratory of Anti-Cancer Drug Research, College of Pharmaceutical Sciences, Zhejiang University, Hangzhou 310058, P. R. China; Innovation Institute for Artificial Intelligence in Medicine of Zhejiang University, Hangzhou 310018, P. R. China*

Complete contact information is available at: https://pubs.acs.org/10.1021/acs.jmedchem.1c00586

Author Contributions

J.C., Z.J., F.Y., and J.Y. contributed equally to this work. J.C. designed and synthesized the compounds, analyzed the data, and drafted the manuscript. Z.J., J.X., B.C., and G.C. synthesized the compounds. F.Y. and J.Y. performed the biological experiments. H.Z., Q.H., Y.H., B.Y., J.C., and X.D. conceived the study and helped analyze the data.

Funding

Key R&D Program of Zhejiang Province; National Natural Science Foundation of China; National Natural Science Foundation for Distinguished Young Scholar of China.

Notes

The authors declare no competing financial interest.

ACKNOWLEDGMENTS

The authors thank Jianyang Pan (Research and Service Center, College of Pharmaceutical Sciences, Zhejiang University) for performing NMR spectrometry for structure elucidation. Figure 8H and Table of Contents Graphic were created with BioRender.com. This work was supported by a grant from the Key R&D Program of Zhejiang Province (2020C03010), the National Natural Science Foundation of China (81673294), and the National Natural Science Foundation for Distinguished Young Scholar of China (81625024).

ABBREVIATIONS

AUC, area under curve; DBU, 1,8-diazabicyclo[5.4.0]undec-7-ene; DCM, dichloromethane; DMAP, 4-dimethylaminopyridine; DMF, dimethylformamide; DMSO, dimethyl sulfoxide; EDCI, 1-ethyl-3-(3′-dimethylaminopropyl) carbodiimide hydrochloride; HOBt, 1-hydroxybenzotriazole; MC, methyl cellulose; m-CPBA, 3-chloroperoxybenzoic acid; RT-PCR, real-time polymerase chain reaction; TMEDA, *N*,*N*,*N*′,*N*′-tetramethylethylenediamine; TEA, triethylamine; THF, tetrahydrofuran

REFERENCES

(1) Valastyan, S.; Weinberg, R. A. Tumor metastasis: molecular insights and evolving paradigms. *Cell* **2011**, *147*, 275−292.

(2) van Zijl, F.; Krupitza, G.; Mikulits, W. Initial steps of metastasis: cell invasion and endothelial transmigration. *Mutat. Res., Rev. Mutat. Res.* **2011**, *728*, 23−34.

(3) Semenza, G. L. Oxygen sensing, hypoxia-inducible factors, and disease pathophysiology. *Annu. Rev. Pathol.: Mech. Dis.* **2014**, *9*, 47−71.

(4) Wilson, W. R.; Hay, M. P. Targeting hypoxia in cancer therapy. *Nat. Rev. Cancer* **2011**, *11*, 393−410.

(5) Archange, C.; Nowak, J.; Garcia, S.; Moutardier, V.; Calvo, E. L.; Dagorn, J. C.; Iovanna, J. L. The WSB1 gene is involved in pancreatic cancer progression. *PLoS One* **2008**, *3*, No. e2475.

(6) Kim, J. J.; Lee, S. B.; Jang, J.; Yi, S. Y.; Kim, S. H.; Han, S. A.; Lee, J. M.; Tong, S. Y.; Vincelette, N. D.; Gao, B.; Yin, P.; Evans, D.; Choi, D. W.; Qin, B.; Liu, T.; Zhang, H.; Deng, M.; Jen, J.; Zhang, J.; Wang, L.; Lou, Z. WSB1 promotes tumor metastasis by inducing pVHL degradation. *Genes Dev.* **2015**, *29*, 2244.

(7) Kim, J. J.; Lee, S. B.; Yi, S. Y.; Han, S. A.; Kim, S. H.; Lee, J. M.; Tong, S. Y.; Yin, P.; Gao, B. W.; Zhang, J.; Lou, Z. K. WSB1 overcomes oncogene-induced senescence by targeting ATM for degradation. *Cell Res.* **2017**, *27*, 274.

(8) Choi, D. W.; Seo, Y. M.; Kim, E. A.; Sung, K. S.; Ahn, J. W.; Park, S. J.; Lee, S. R.; Choi, C. Y. Ubiquitination and degradation of homeodomain-interacting protein kinase 2 by WD40 repeat/SOCS box protein WSB-1. *J. Biol. Chem.* **2008**, *283*, 4682.

(9) Cao, J.; Wang, Y.; Dong, R.; Lin, G.; Zhang, N.; Wang, J.; Lin, N.; Gu, Y.; Ding, L.; Ying, M.; He, Q.; Yang, B. Hypoxia-induced WSB1 promotes the metastatic potential of osteosarcoma cells. *Cancer Res.* **2015**, *75*, 4839−4851.

(10) Gildea, J. J.; Seraj, M. J.; Oxford, G.; Harding, M. A.; Hampton, G. M.; Moskaluk, C. A.; Frierson, H. F.; Conaway, M. R.; Theodorescu, D. RhoGD12 is an invasion and metastasis suppressor gene in human cancer. *Cancer Res.* **2002**, *62*, 6418−6423.

(11) Harding, M. A.; Theodorescu, D. RhoGDI2: a new metastasis suppressor gene: discovery and clinical translation. *Urol. Oncol.: Semin. Orig. Invest.* **2007**, *25*, 401−406.

(12) Agarwal, N. K.; Chen, C. H.; Cho, H.; Boulbes, D. R.; Spooner, E.; Sarbassov, D. D. Rictor regulates cell migration by suppressing RhoGDI2. *Oncogene* **2013**, *32*, 2521.

(13) Warchal, S. J.; Unciti-Broceta, A.; Carragher, N. O. Next-generation phenotypic screening. *Future Med. Chem.* **2016**, *8*, 1331.

(14) Vincent, F.; Loria, P. M.; Weston, A. D.; Steppan, C. M.; Doyonnas, R.; Wang, Y. M.; Rockwell, K. L.; Peakman, M. C. Hit triage and validation in phenotypic screening: considerations and strategies. *Cell Chem. Biol.* **2020**, *27*, 1332.

(15) Sato, M. Phenotypic screening using large-scale genomic libraries to identify drug targets for the treatment of cancer. *Oncol. Lett.* **2020**, *19*, 3617−3626.

(16) Brito, H.; Marques, V.; Afonso, M. B.; Brown, D. G.; Borjesson, U.; Selmi, N.; Smith, D. M.; Roberts, I. O.; Fitzek, M.; Aniceto, N.; Guedes, R. C.; Moreira, R.; Rodrigues, C. M. P. Phenotypic high-throughput screening platform identifies novel chemotypes for necroptosis inhibition. *Cell Death Discovery* **2020**, *6*, No. 6.

(17) Zhang, B.; Guo, R. Y.; Hu, Y. Z.; Dong, X. W.; Lin, N. M.; Dai, X. Y.; Wu, H. H.; Ma, S. L.; Yang, B. Design, synthesis and biological evaluation of valepotriate derivatives as novel antitumor agents. *RSC Adv.* **2017**, *7*, 31899−31906.

(18) Wang, S.; Jin, R.; Wang, R.; Hu, Y.; Dong, X.; Xu, A. The design, synthesis and biological evaluation of pro-EGCG derivatives as novel anti-vitiligo agents. *RSC Adv.* **2016**, *6*, 106308−106315.

(19) Weng, Q. J.; Che, J. X.; Zhang, Z. K.; Zheng, J. H.; Zhan, W. H.; Ling, S. D.; Tian, T.; Wang, J. C.; Gai, R. H.; Hu, Y. Z.; Yang, B.; He, Q. J.; Dong, X. W. Phenotypic screening-based identification of 3,4-disubstituted piperidine derivatives as macrophage M2 polarization modulators: an opportunity for treating multiple sclerosis. *J. Med. Chem.* **2019**, *62*, 3268−3285.

(20) Che, J. X.; Wang, Z. L.; Dong, X. W.; Hu, Y. H.; Xie, X.; Hu, Y. Z. Bicyclo[2.2.1]heptane containing N,N-diarylsquaramide CXCR2 selective antagonists as anti-cancer metastasis agents. *RSC Adv.* **2018**, *8*, 11061−11069.

(21) Che, J.; Wang, Z.; Sheng, H.; Huang, F.; Dong, X.; Hu, Y.; Xie, X.; Hu, Y. Ligand-based pharmacophore model for the discovery of novel CXCR2 antagonists as anti-cancer metastatic agents. *R. Soc. Open Sci.* **2018**, *5*, No. 180176.

(22) Dong, X. W.; Zhan, W. H.; Zhao, M. T.; Che, J. X.; Dai, X. Y.; Wu, Y. Z.; Xu, L.; Zhou, Y. B.; Zhao, Y. M.; Tian, T.; Chen, G.; Jin, Z. G.; Li, J.; Shao, Y. F.; He, Q. J.; Yang, B.; Weng, Q. J.; Hu, Y. Z. Discovery of 3,4,6-trisubstituted piperidine derivatives as orally active, low hERG blocking Akt inhibitors via conformational restriction and structure-based design. *J. Med. Chem.* **2019**, *62*, 7264−7288.

(23) Dovas, A.; Couchman, J. R. RhoGDI: multiple functions in the regulation of Rho family GTPase activities. *Biochem. J.* **2005**, *390*, 1−9.

https://doi.org/10.1021/acs.jmedchem.1c00586
J. Med. Chem. 2021, 64, 8621−8643